

Seasonal variability of nitrous oxide concentrations and emissions in a temperate estuary

Gesa Schulz^{1,2}, Tina Sanders², Yoana G. Voynova², Hermann W. Bange³, and Kirstin Dähnke²

¹Institute of Geology, Center for Earth System Research and Sustainability (CEN), University Hamburg, Hamburg, 20146, Germany

²Institute of Carbon Cycles, Helmholtz Centre Hereon, Geesthacht, 21502, Germany

³Marine Biogeochemistry Research Division, GEOMAR Helmholtz Centre for Ocean Research Kiel, Kiel, 24105, Germany

Correspondence to: Gesa Schulz (Gesa.Schulz@hereon.de)

Abstract

Nitrous oxide (N₂O) is a greenhouse gas, with a global warming potential 298 times that of carbon dioxide. Estuaries can be sources of N₂O, but their emission estimates have significant uncertainties due to limited data availability and high spatiotemporal variability. We investigated the spatial and seasonal variability of dissolved N₂O and its emissions along the Elbe Estuary (Germany), a well-mixed temperate estuary with high nutrient loading from agriculture. During nine research cruises performed between 2017 and 2022, we measured dissolved N₂O concentrations, as well as dissolved nutrients and oxygen concentrations along the estuary and calculated N₂O saturations, flux densities and emissions. We found that the estuary was a year-round source of N₂O, with highest emissions in winter when dissolved inorganic nitrogen (DIN) loads and wind speeds are high. However, in spring and summer, N₂O saturations and emissions did not decrease alongside lower riverine nitrogen loads, suggesting that estuarine in-situ N₂O production is an important source of N₂O. We identified two hot-spots areas of N₂O production: the Port of Hamburg, a major port region, and the mesohaline estuary near the maximum turbidity zone (MTZ). N₂O production was enhanced by warmer temperatures and was fueled by decomposition of riverine organic matter in the Hamburg Port and by marine organic matter in the MTZ. A comparison with previous measurements in the Elbe Estuary revealed that N₂O saturation did not decrease alongside with DIN concentrations after a significant improvement of water quality in the 1990s that allowed for phytoplankton growth to reestablish in the river and estuary. This effect of phytoplankton growth and the overarching control of organic matter on N₂O production, highlights that eutrophication and agricultural nutrient input can increase N₂O emissions in estuaries.

1 Introduction

Nitrous oxide (N₂O) is an important atmospheric trace gas that contributes to global warming and stratospheric ozone depletion (WMO, 2018; IPCC, 2021). Estuaries are important regions of nitrogen turnover (Middelburg and Nieuwenhuize, 2000; Crossland et al., 2005; Bouwman et al., 2013), and a potential source of N₂O (Bange, 2006; Barnes and Upstill-Goddard, 2011; Murray et al., 2015). Together with coastal wetlands, estuaries contribute between 0.17 and 0.95 Tg N₂O-N of the annual global budget of 16.9 Tg N₂O-N (Murray et al., 2015; Tian et al., 2020). N₂O emission estimates from estuaries are associated with significant uncertainties due to limited data availability and high spatiotemporal variability (e.g. Bange, 2006; Barnes and Upstill-Goddard, 2011; Maavara et al., 2019), presenting a big challenge for the global N₂O emission estimates.

39 Nitrification and denitrification are the most important N_2O production pathways in estuaries. Under oxic
40 conditions, N_2O is produced as a side product during the first step of nitrification, the oxidation of ammonia to
41 nitrite (e.g. Wrage et al., 2001; Barnes and Upstill-Goddard, 2011). At low oxygen (but not anoxic) conditions,
42 nitrifier-denitrification may occur, during which nitrifiers reduce nitrite to N_2O (e.g. Wrage et al., 2001; Bange,
43 2008). Denitrification takes place under anoxic conditions and mostly acts as a source of N_2O , but can also reduce
44 N_2O to N_2 (e.g. Knowles, 1982; Bange, 2008). In estuaries, denitrification can occur in anoxic sediments, the
45 anoxic water column or anoxic microsites of particles, whereas nitrification and nitrifier-denitrification take place
46 in the oxygenated water column (Beaulieu et al., 2010; Murray et al., 2015; Ji et al., 2018; Tang et al., 2022).
47 In estuaries, the most important factor controlling N_2O emissions are considered to be oxygen availability and
48 dissolved inorganic nitrogen loads (Murray et al., 2015). Since N_2O measurements in estuaries are scarce, global
49 N_2O emissions can be estimated by using emission factors and considering dissolved inorganic nitrogen (DIN) or
50 total nitrogen (TN) loads, where it is assumed that higher loads lead to higher N_2O emissions (Kroeze et al., 2005,
51 2010; Ivens et al., 2011; Hu et al., 2016). However, several studies instead reported no obvious relationship
52 between nitrogen concentrations and N_2O emissions (Borges et al., 2015; Marzadri et al., 2017; Wells et al., 2018),
53 highlighting the need to understand the causes for variability of the relationship between nitrogen loads and N_2O
54 emissions (Wells et al., 2018).
55 The Elbe Estuary is a heavily managed estuary with high agricultural nitrogen inputs that hosts the third largest
56 port in Europe (e.g. Radach and Pätsch, 2007; Bergemann and Gaumert, 2008; Pätsch et al., 2010; Quiel et al.,
57 2011). It has been identified as a N_2O source, with a hotspot of N_2O production in the Port of Hamburg (Hanke
58 and Knauth, 1990; Brase et al., 2017). We aimed to investigate drivers for N_2O emissions along the estuary,
59 specifically the N_2O and DIN ratio ($\text{N}_2\text{O}:\text{DIN}$). To do so, we (1) looked for potential long-term changes in N_2O
60 saturations, (2) investigated potential production hotspots as well as the spatial and temporal distribution of N_2O
61 saturations, and (3) used the $\text{N}_2\text{O}:\text{DIN}$ ratio for a comparison with other estuaries that receive similar high
62 agricultural nutrient inputs.

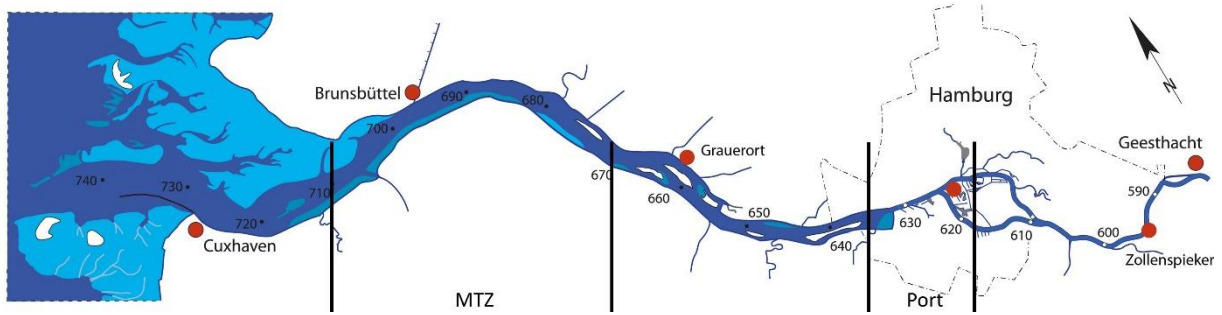
63 **2 Methods**

64 **2.1 Study site**

65 The Elbe River stretches over 1094 km from the Giant Mountains (Czech Republic) to the North Sea (Cuxhaven,
66 Germany). The catchment of the Elbe River is 140 268 km² (Boehlich and Strotmann, 2019), with 74 % urban and
67 agricultural land-use (Johannsen et al., 2008). The Elbe is the second largest German river discharging into the
68 North Sea, as well as the largest source of dissolved nitrogen for the German Bight, which is heavily affected by
69 eutrophication (van Beusekom et al., 2019).

70 The Elbe Estuary is a well-mixed temperate estuary, which begins at stream kilometer 586 at a weir in Geesthacht
71 and stretches through the Port of Hamburg, entering the North Sea near Cuxhaven at stream kilometer 727 (Fig.
72 1). Estuaries are commonly structured along their salinity gradient into an oligohaline (salinity: 0.5 – 5.0), a
73 mesohaline (salinity: 5.0 – 18.0) and polyhaline (salinity > 18.0) (US EPA, 2006). The Elbe Estuary has a length
74 of 142 km (Boehlich and Strotmann, 2019) and a mean annual discharge of 712 m³ s⁻¹ (measured at gauge Neu
75 Darchau at stream kilometer 536; HPA and Freie und Hansestadt Hamburg, 2017). The average water residence
76 time is ~32 days, ranging from ~72 days during times of low discharge (300 m³ s⁻¹) to ~10 days during times of
77 high discharge (2000 m³ s⁻¹; Boehlich and Strotmann, 2008). The estuary has an annual nitrogen load of 84 Gg-N

78 (FGG Elbe, 2018). Point sources along the estuary provide only small part of the total nitrogen input to the Elbe
 79 Estuary (Hofmann et al., 2005; IKSE, 2018). Oxygen concentrations in the Elbe Estuary vary seasonally, with
 80 oxygen depletion during the summer months and oxygen minimum zones regularly experiencing concentrations
 81 below $94 \mu\text{mol O}_2 \text{L}^{-1}$ (Schroeder, 1997; Gaumert and Bergemann, 2007; Schöl et al., 2014).
 82 The Elbe Estuary is dredged year-round to maintain a water depth of 15 – 20 m and to grant access for large
 83 container ships to the Port of Hamburg (Boehlich and Strotmann, 2019; Hein et al., 2021). Construction work for
 84 further deepening of the fairway was carried out during our study period, from 2019 to early 2022. Upstream of
 85 the Port of Hamburg water depth is less than 10 m (Hein et al., 2021).



86
 87 **Figure 1: Map of the Elbe Estuary sampled during our research cruises with stream kilometers. The vertical black lines**
 88 **indicate the Hamburg Port region and a typical position for the maximum turbidity zone (MTZ, Bergemann, 2004).**

89 **2.2 Transect sampling and measurements**

90 We performed nine sampling campaigns along the estuary with the research vessel *Ludwig Prandtl* (Table 1). Most
 91 cruises took place during spring and summer, with water temperatures $> 10 \text{ }^\circ\text{C}$ (May to September), two cruises
 92 were conducted during winter (early March, water temperature $< 6 \text{ }^\circ\text{C}$; Table 1). Transects started in the German
 93 Bight, and continued along the salinity gradient, through the Port of Hamburg to Oortkaten (stream kilometer
 94 609). To ensure comparable current and mixing conditions, transect sampling was always done after high-tide,
 95 with the ship travelling upstream against the tide. For comparison to previous measurements, we included summer
 96 data from a previous study in 2015 (Brase et al., 2017).

97 **Table 1: Campaign dates with the sampled Elbe Estuary sections shown via stream kilometers, average discharge**
 98 **during each cruise measured at the Neu Darchau gauging station, averages and standard deviations for water**
 99 **temperature, wind speed at 10 m height, dissolved inorganic nitrogen (DIN) concentrations for each campaign.**

Campaign Dates	Stream kilometers (km)	Water temperature (°C)	Wind speed 10 m (m s ⁻¹)	Average discharge (m ³ s ⁻¹)	Average DIN load (μmol L ⁻¹)
28.-29.04.2015	627 – 741	12.3 ± 1.0	7.4 ± 2.3	595	191.0 ± 45.0
02.-04.06.2015	609 – 739	17.4 ± 1.7	5.0 ± 1.3	276	105.9 ± 36.2
01.-02.08.2017	621 – 749	20.9 ± 0.7	3.6 ± 1.5	607	79.2 ± 30.2
04.-05.06.2019	610 – 750	18.7 ± 2.2	4.0 ± 1.7	423	108.3 ± 35.9
30.07.-01.08.2019	609 – 752	22.6 ± 1.0	4.2 ± 1.4	171	60.8 ± 38.6
19.-20.06.2020	609 – 747	19.8 ± 1.4	5.8 ± 1.2	331	74.6 ± 33.8
09.-11.09.2020	607 – 745	18.9 ± 0.6	5.9 ± 2.8	305	93.1 ± 32.7
10.-12.03.2021	609 – 748	5.4 ± 0.5	9.3 ± 2.6	862	324.4 ± 83.8
04.-05.05.2021	610 – 751	10.5 ± 0.8	11.0 ± 3.1	411	85.7 ± 36.6
27.-28.07.2021	621 – 751	22.2 ± 0.7	5.2 ± 1.3	721	139.8 ± 58.4
01.-02.03.2022	610 – 752	5.6 ± 0.2	2.9 ± 1.0	1282	238.0 ± 74.7

100 An onboard membrane pump continuously provided water at 1.2 m depth to an on-line in-situ FerryBox system
 101 and to an equilibrator used for the measurements of N₂O dry mole fraction (Section 2.4). The FerryBox system
 102 continuously measured water temperature, salinity, oxygen concentrations, pH and turbidity. We corrected the
 103 salinity corrected optode measurements using comparisons to Winkler titrations of distinct samples. See Table S1
 104 for further details.

105 Discrete water samples (30-40 samples for each cruise) were collected every 20 min from a bypass of the FerryBox
 106 system. For nutrient analysis, water samples were filtered immediately through combusted, pre-weighted GF/F
 107 Filters (4 h, 450 °C), and were frozen in acid washed PE-bottles until analysis. The filters were also stored frozen
 108 (-20 °C) and subsequently analyzed for suspended particulate matter (SPM), particulate nitrogen (PN), particulate
 109 carbon (PC) and C/N ratios (Fig. S1).

110 **2.3 Nutrient measurements**

111 Filtered water samples were measured in triplicates with a continuous flow auto analyzer (AA3, SEAL Analytics)
 112 using standard colorimetric and fluorometric methods (Hansen and Koroleff, 1999) for dissolved nitrate (NO₃⁻),
 113 nitrite (NO₂⁻) and ammonium (NH₄⁺) concentrations. Detection limits were 0.05 μmol L⁻¹, 0.05 μmol L⁻¹, and
 114 0.07 μmol L⁻¹ for nitrate, nitrite and ammonium, respectively.

115 **2.4 Equilibrator based N₂O measurements and calculations**

116 Equilibrated dry mole fractions of N₂O were measured by an N₂O analyzer based on off-axis integrated cavity
 117 output (OA-ICOS) absorption spectroscopy (Model 914-0022, Los Gatos Res. Inc., San Jose, CA, USA), which
 118 was coupled with a sea water/gas equilibrator using off-axis cavity output spectroscopy. Brase et al. (2017)
 119 described the set-up and instrument precision in detail. Twice a day, two standard gas mixtures of N₂O in synthetic
 120 air (500.5 ppb ± 5 % and 321.2 ppb ± 3 %) were analyzed to validate our measurements. No drift was detected
 121 during our cruises.

122 We calculated the dissolved N₂O concentrations in water with the Bunsen solubility function of Weiss and Price
 123 (1980), using 1 min averages of the measured N₂O dry mole fraction (ppb). Temperature differences between the
 124 sample inlet and the equilibrator were taken into account for the calculation of the final N₂O concentrations Rhee
 125 et al. (2009). N₂O saturation were calculated based on N₂O concentrations in water (N₂O_{cw}) and the atmospheric
 126 equilibration concentrations (N₂O_{eq}; Eq. 1). Atmospheric N₂O dry mole fractions were measured before and after
 127 each transect cruises using an air duct from the deck of the research vessel.

$$s = 100 \times \frac{N_2O_{cw}}{N_2O_{eq}} \quad (1)$$

128 The gas transfer coefficients (k) were determined based on Borges et al. (2004, Eq. 3), Nightingale et al. (2000),
 129 Wanninkhof (1992) and Clark et al. (1995), using the Schmidt number (Sc) and wind speeds (u₁₀) measured at
 130 10 m height (Eq. 2). The Schmidt number was calculated as ratio of the kinematic viscosity in water (Siedler and
 131 Peters, 1986) to the N₂O diffusivity in water (Rhee, 2000). Cruise wind speeds (Table 1) varied significantly from
 132 average annual wind speeds of the two federal states, in which the Elbe Estuary is located (4.7 m s⁻¹, Schleswig-
 133 Holstein u. Hamburg: Mittlere Windgeschwindigkeit (1986-2015)* | Norddeutscher Klimamonitor, 2023), and
 134 also compared to seasonal average wind speeds determined for the stations Cuxhaven and Hamburg (Rosenhagen
 135 et al., 2011). Thus, to estimate uncertainties due to varying wind conditions during our cruises, we used 1) the
 136 in-situ wind speeds measured on board the *R/V Ludwig Prandtl* at 10 m height by a MaxiMet GMX600 (Gill
 137 Instruments Limited, Hampshire, UK), 2) the average annual wind speed (Schleswig-Holstein u. Hamburg:
 138 Mittlere Windgeschwindigkeit (1986-2015)* | Norddeutscher Klimamonitor, 2023), and 3) the seasonally
 139 averaged wind speeds (Rosenhagen et al., 2011). The flux densities in the main text were calculated using Eq. 3
 140 and the wind speeds measured on board the vessel. Results of the other calculations are listed in the supplementary
 141 material (Table S2).

$$k = 0.24 \times (4.045 + 2.58u_{10}) \times \left(\frac{Sc}{600}\right)^{-0.5} \quad (2)$$

$$f = k \times (N_2O_{cw} - N_2O_{air}) \quad (3)$$

142 To estimate N₂O emissions, we separated the Elbe Estuary into five regions: limnic (stream kilometer 585 to 615),
 143 Port of Hamburg (stream kilometer 615 to 632), oligohaline (stream kilometer 632 to 704), mesohaline (stream
 144 kilometer 704 – 727) and polyhaline (stream kilometer 727 to 750), see Table S3. Respective areas were provided
 145 by the German Federal Waterways Engineering and Research Institute (BAW, pers. Comm., Ortiz, 2023) and
 146 Geerts et al. (2012). In order to account for seasonality, cruises were defined as: winter (March), spring (April and
 147 May), summer (June and July) and late summer/autumn (August and September). We then calculated daily N₂O
 148 emissions per section and season. For upscaling, we used calculated monthly emissions to estimate annual
 149 emissions (winter: November to March, spring: April to May, summer: June to July and late summer/autumn:
 150 August to October). To address uncertainties, we calculated N₂O emissions based on different parametrizations
 151 and wind speeds as described above.

152 2.5 Excess N₂O and apparent oxygen utilization

153 The correlation between excess N₂O (N₂O_{xs}) and apparent oxygen utilization (AOU) can provide insights into N₂O
 154 production (Nevison et al., 2003; Walter et al., 2004). We calculated N₂O_{xs} as the difference between the N₂O
 155 concentration in water (N₂O_w) and the theoretical equilibrium concentration (N₂O_{eq}) (Eq. 4). AOU was determined

156 using Eq. 5, where O_2 is the measured dissolved oxygen concentration, and O_2' is the theoretical equilibrium
157 concentration between water and atmosphere calculated according to Weiss (1970).

$$N_2O_{xs} = N_2O_w - N_2O_{eq} \quad (4)$$

$$AOU = O_2' - O_2 \quad (5)$$

158 A linear relationship between AOU and N_2O_{xs} is usually an indicator for nitrification (Nevison et al., 2003; Walter
159 et al., 2004).

160 **2.6 Statistical analysis**

161 All statistical analyses were done using R packages. The packages ggpubr v.0.6.0 (Kassambara, 2023) and stats
162 v.4.0.2 (The R Stats Package, Version 4.0.2, 2021) were used to calculate Pearson correlations (R) and p-values.

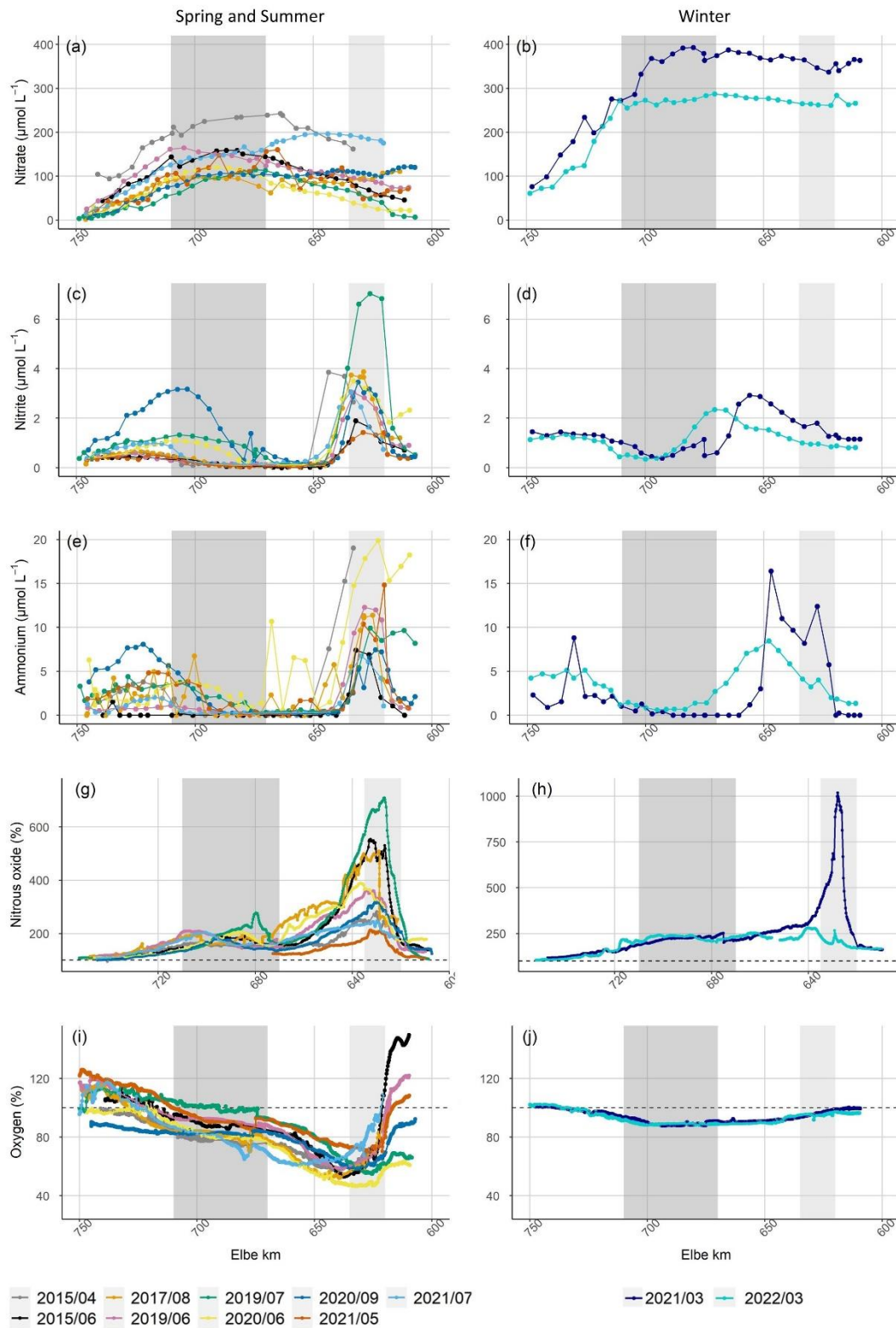
163 **3 Results**

164 **3.1 Hydrographic properties and DIN distribution**

165 Discharge ranged between $171 \text{ m}^3 \text{ s}^{-1}$ and $1282 \text{ m}^3 \text{ s}^{-1}$ during our cruises (ZDM, 2022), with higher discharge in
166 winter and lower discharge in summer (Table 1). Average water temperature over the entire estuary ranged from
167 $5.4 \pm 0.5 \text{ }^\circ\text{C}$ in March 2021 to $22.6 \pm 1.0 \text{ }^\circ\text{C}$ in August 2017 (Table 1). For further evaluation, March 2021 and
168 2022 cruises were regarded as winter cruises (water temperature $< 6^\circ\text{C}$), whereas all cruises with higher water
169 temperature were jointly regarded as spring and summer conditions.

170 Nitrate was the major form of dissolved inorganic nitrogen (DIN) during all cruises. In winter, high nitrogen
171 concentrations entered the estuary from the river. Towards summer, the riverine input of nitrate (stream kilometer
172 < 620) decreased, but along the estuary nitrate concentrations increased up to ~stream kilometer 700, then
173 decreased towards the North Sea. Nitrate concentrations were highest during both March cruises with averages of
174 $319.0 \pm 85.7 \text{ } \mu\text{mol L}^{-1}$ and $230.9 \pm 76.2 \text{ } \mu\text{mol L}^{-1}$ in 2021 and 2022, respectively. During summer, nitrate
175 concentrations were lower, with averages between $151.0 \pm 58.1 \text{ } \mu\text{mol L}^{-1}$ in May 2021 and $63.3 \pm 38.8 \text{ } \mu\text{mol L}^{-1}$
176 in July 2019 (Fig. 2a and b).

177 Nitrite and ammonium concentrations were usually low ($< 1 \text{ } \mu\text{mol L}^{-1}$) throughout the Elbe Estuary, but peaked
178 in the Hamburg Port region and around stream kilometer 720 (Fig. 2c and 2e). We measured pronounced variations
179 in nitrite concentrations during most of our cruises, ranging from $> 6.0 \text{ } \mu\text{mol L}^{-1}$ (July 2019) to concentrations
180 below the detection limit (Fig. 2c and d). The highest ammonium concentration was measured in March 2021 at
181 $23.5 \text{ } \mu\text{mol L}^{-1}$ (Fig. 2e and f).



182

183 **Figure 2: Nitrate concentration along the Elbe Estuary (a) in spring/summer, (b) in winter. Nitrite concentration along**
 184 **the Elbe Estuary (c) in spring/summer and (d) in winter. Ammonium concentration along the Elbe Estuary (e) in**
 185 **spring/summer and (f) in winter. N_2O in % saturation along the Elbe Estuary (g) in spring/summer, (h) in winter.**
 186 **Dissolved oxygen in % saturation along the Elbe Estuary (i) in spring/summer and (j) in winter. All variables are plotted**
 187 **against Elbe stream kilometers (Elbe km). Light grey shading denotes the Hamburg Port region, dark grey shading the**
 188 **typical position of the maximum turbidity zone (MTZ, Bergemann, 2004). Note the difference in Y-axis scales for the**
 189 **plots of (g) and (h). The dashed black lines in (g) and (h), as well as (i) and (j) indicate saturation of 100 % for nitrous**
 190 **oxide and dissolved oxygen, respectively.**

191 **3.2 Atmospheric N₂O and N₂O saturation**

192 The average atmospheric N₂O dry mole fractions ranged from 325 ppb in June 2015 to 336 ppb in July 2022 (Table
 193 2). The differences between our measurements and the mean monthly N₂O mole fraction measured at the Mace
 194 Head atmospheric monitoring station (Ireland; Dlugokencky et al., 2022) were always less than 1.5 %, indicating
 195 a good agreement with the monitoring data.

196 During all cruises, the Elbe Estuary was supersaturated in N₂O in the freshwater region (Fig. 2g, h). The average
 197 N₂O saturation over the entire transect ranged between 146 % and 243 % with an overall average of 197 % for all
 198 cruises. Highest N₂O occurred in the Hamburg Port region in spring and summer with an average N₂O peak of
 199 402 % saturation and a maximum supersaturation of 710 % in July 2019. The distributions of N₂O during winter
 200 cruises were significantly different: In March 2022, highest N₂O (280 % saturation) occurred at stream kilometer
 201 640. In contrast, in March 2021, we found an extraordinarily high peak with a saturation of 1018 % at stream
 202 kilometer 627. Between stream kilometer 680 and 720, a supersaturation of up to 277 % occurred in spring and
 203 summer. Further towards the North Sea, N₂O decreased, approaching equilibrium with the atmosphere.

204 **3.3 N₂O flux densities and N₂O emissions**

205 For N₂O flux densities, we in the following present calculated values after Borges et al. (2004, Table 2). See Table
 206 S2 for results of other parametrizations. The N₂O flux densities were usually highest in the Hamburg Port area,
 207 with an average of $95.0 \pm 97.9 \mu\text{mol m}^{-2} \text{d}^{-1}$ and lowest towards the North Sea, with an average of
 208 $3.9 \pm 3.0 \mu\text{mol m}^{-1} \text{d}^{-1}$ (Elbe stream kilometers > 735). The average N₂O flux density of all cruises was
 209 $39.9 \pm 46.9 \mu\text{mol m}^{-2} \text{d}^{-1}$ (calculated with in-situ wind speeds measured during the cruises).

210 **Table 2: Calculated average N₂O saturation, sea-to-air fluxes calculated following Borges et al. (2004) and atmospheric**
 211 **N₂O dry mole fractions during our cruises in the Elbe Estuary**

Campaign Dates	Average saturation (%)	N ₂ O Flux densities ($\mu\text{mol m}^{-2} \text{d}^{-1}$)			Average atmospheric dry mole fraction (ppb)
		In-situ wind	Annual wind	Seasonal wind	
28.-29.04.15	160.8 ± 37.9	33.1 ± 21.0	23.1 ± 14.7	25.4 ± 16.1	331 ± 0.5
02.-04.06.15	203.8 ± 112.7	39.0 ± 42.7	37.2 ± 40.7	37.8 ± 41.4	325 ± 0.8
01.-02.08.17	221.0 ± 106.5	35.6 ± 31.8	43.2 ± 38.5	44.1 ± 39.3	331 ± 1.2
04.-05.06.19	192.6 ± 66.0	29.7 ± 21.5	33.5 ± 24.2	34.0 ± 24.6	332 ± 0.2
30.07.-01.08.19	232.5 ± 155.3	42.0 ± 50.1	45.7 ± 54.5	47.4 ± 56.4	327 ± 1.0
19.-20.06.20	193.9 ± 74.1	39.2 ± 31.6	33.3 ± 26.9	33.9 ± 27.3	330 ± 0.6
09.-11.09.20	160.5 ± 53.6	26.0 ± 23.5	21.8 ± 19.7	24.5 ± 22.1	331 ± 0.7
10.-12.03.21	242.5 ± 141.6	100.7 ± 101.2	58.1 ± 58.4	71.0 ± 71.4	331 ± 1.3
04.-05.05.21	145.6 ± 28.8	35.6 ± 22.5	17.8 ± 11.2	18.5 ± 11.7	331 ± 0.8
27.-28.07.21	172.6 ± 37.2	28.0 ± 14.6	25.9 ± 13.6	26.9 ± 14.1	334 ± 3.8
01.-02.03.22	196.5 ± 47.0	27.8 ± 13.9	39.0 ± 19.5	47.7 ± 23.8	333 ± 0.7

212
 213 N₂O emission estimates varied significantly depending on the used parametrization and wind speeds. Note that we
 214 calculated emission twice: 1) including (w 03/2021) and 2) deliberately excluding (w/o 03/2021) the N₂O peak
 215 saturation measured in the Port of Hamburg in March 2021, using a linear interpolated concentrations in the
 216 respective. Highest emissions were calculated following methods by Borges et al. (2004) and using in-situ wind

217 speeds, resulting in emissions of 0.25 ± 0.16 Gg-N₂O yr⁻¹ and 0.23 ± 0.12 Gg-N₂O yr⁻¹ with and without the N₂O
 218 peak in March 2021, respectively. Lowest emissions of 0.08 Gg-N₂O yr⁻¹ arose with parametrization of Nightingale
 219 et al. (2000) and Wanninkhof (1992), and using annual wind speeds (Table 3).

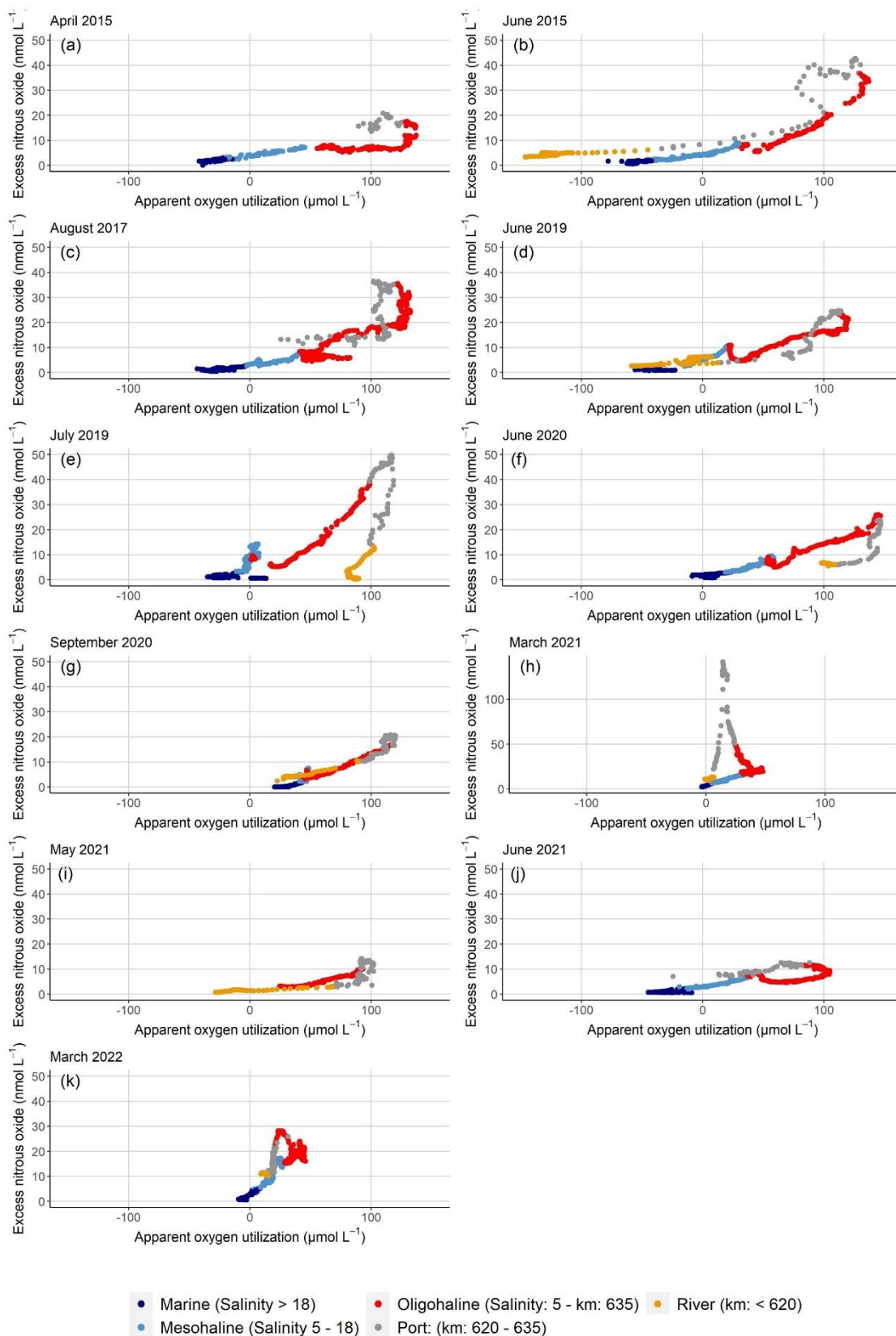
220 **Table 3: Annual N₂O emission estimates in Gg-N₂O yr⁻¹ calculated with different parametrizations and wind speeds**

		Emissions in Gg-N ₂ O yr ⁻¹			
		Borges et al. (2004)	Nightingale et al. (2000)	Wanninkhof (1992)	Clark et al. (1995)
w	In-situ wind	0.25 ± 0.16	0.14 ± 0.12	0.17 ± 0.15	0.16 ± 0.12
03/2021	Annual wind	0.21 ± 0.11	0.08 ± 0.04	0.09 ± 0.05	0.09 ± 0.05
	Seasonal wind	0.24 ± 0.12	0.11 ± 0.06	0.13 ± 0.06	0.12 ± 0.06
w/o	In-situ wind	0.23 ± 0.12	0.13 ± 0.09	0.15 ± 0.11	0.14 ± 0.09
03/2021	Annual wind	0.20 ± 0.08	0.08 ± 0.03	0.08 ± 0.03	0.09 ± 0.04
	Seasonal wind	0.22 ± 0.09	0.11 ± 0.04	0.12 ± 0.04	0.12 ± 0.04

221 3.4 Dissolved oxygen saturation

222 Average oxygen varied between 76 and 95 % saturation with an oxygen minimum in the Hamburg Port area.
 223 Winter cruises varied little, with oxygen remaining relatively constant along the estuary (> 88 % saturation).
 224 During most spring and summer cruises, water from the river coming into the estuary was supersaturated in oxygen
 225 (> 100 % saturation). In the Hamburg Port region, oxygen saturation generally decreased. Lowest values occurred
 226 in June 2020 with 47 % saturation. The along-estuary oxygen minimum in summer months (June to August) was
 227 always below 61 % saturation. In spring and summer, oxygen increased towards the North Sea and reached
 228 100 % saturation (Fig. 2i and j).

229 Plots of excess N₂O (N₂O_{xs}) and apparent oxygen utilization (AOU) revealed excess N₂O along the entire estuary
 230 (Fig. 3). During all cruises, elevated riverine N₂O_{xs} entered the estuary (stream kilometer < 620). A linear positive
 231 relationship between N₂O_{xs} and AOU suggested nitrification as main production pathway in large sections of the
 232 estuary (Nevison et al., 2003; Walter et al., 2004). However, in summer, a change of slope in the Port of Hamburg
 233 as well as in the mesohaline section of the estuary suggested either increased in-situ N₂O production or external
 234 N₂O input. In winter, we found an increasing slope in the Hamburg Port region and in the oligohaline part of the
 235 Elbe Estuary (Fig. 3h, k).



236

237 **Figure 3: Plots of N_2O_{xs} vs AOU for (a) April 2015, (b) June 2015, (c) August 2017, (d) June 2019, (e) July 2019, (f) June**
 238 **2020, (g) September 2020, (h) March 2021, (i) May 2021, (j) June 2021 and (k) March 2022. The values are colored to**
 239 **distinguish between different regions of the estuary. Y-axis scale differ for Fig. 3h.**

240 3.5 Statistical analysis

241 We performed a statistical analyses to identify potential N₂O production pathways and controlling factors. Table 4
 242 summarizes the results for the entire data set with further separation into spring and summer cruises (sp/su), as
 243 well as separation according to presence of a salinity gradient (salinity > 1) or freshwater regions (salinity < 1).
 244 Further, we performed corresponding analysis to assess the significance of correlations between for average values
 245 of different parameters for each cruise (Table 5).

246 **Table 4: Pearson correlation coefficients (R) for N₂O saturation (%) with temperature (T in °C), pH value, oxygen (O₂
 247 in %), ammonium concentrations (NH₄⁺ in μmol L⁻¹), nitrite concentrations (NO₂⁻ in μmol L⁻¹), nitrate concentrations
 248 (NO₃⁻ in μmol L⁻¹), SPM concentrations (SPM in mg L⁻¹), C/N values, particulate carbon fraction (PC in %) and
 249 particulate nitrogen fraction (PN in %) for the entire data set, spring and summer cruises (sp/su), data with salinity > 1,
 250 spring and summer cruises with salinity > 1, data with salinity < 1 and spring and summer cruises with salinity < 1. The
 251 significance is shown as ** for p-value < 0.001, * for p-values < 0.01 and + for p-values < 0.05.**

N ₂ O saturation %	T °C	pH	O ₂ %	NH ₄ ⁺ μM	NO ₂ ⁻ μM	NO ₃ ⁻ μM	SPM mg	C/N	PC %	PN %
Entire data	0.06	-0.47**	-0.56**	0.27**	0.48**	0.23	0.10	0.60	-0.05	-0.13 ⁺
sp/su	0.33*	-0.59**	-0.65**	0.23**	0.53**	0.09	0.02	0.24**	-0.09	-0.13 ⁺
Sal>1	0.03	-0.40**	-0.53**	-0.32**	-0.05	0.71**	0.32**	0.11*	-0.24	-0.39**
Sal<1,	0.01	-0.41**	-0.42**	0.28**	0.51**	-0.00	-0.08	0.15	-0.25*	-0.24*
Sal>1, sp/su	-0.10	-0.21 ⁺	-0.52**	-0.28**	0.01	0.62**	0.02	0.39**	-0.31**	-0.41**
Sal<1, sp/su	0.30**	-0.60**	-0.57**	0.21 ⁺	0.58**	-0.23*	-0.16 ⁺	0.11	-0.30*	-0.27*

252
 253 **Table 5: Pearson correlation coefficients (R) for average N₂O saturation (%) with average discharge (Q in m³ s⁻¹)
 254 temperature (T in °C), pH value, oxygen (O₂ in %), ammonium concentrations (NH₄⁺ in μmol L⁻¹), nitrite concentrations
 255 (NO₂⁻ in μmol L⁻¹), nitrate concentrations (NO₃⁻ in μmol L⁻¹), SPM concentrations (SPM in mg L⁻¹), C/N values,
 256 particulate carbon fraction (PC in %) and particulate nitrogen fraction (PN in %) for the entire data set, spring and
 257 summer cruises (sp/su), data with salinity > 1, spring and summer cruises with salinity > 1, data with salinity < 1 and
 258 spring and summer cruises with salinity < 1. The significance is shown as ** for p-value < 0.001, * for p-values < 0.01
 259 and + for p-values < 0.05.**

N ₂ O saturation %	Q m ³ s ⁻¹	T °C	pH	O ₂ %	NH ₄ ⁺ μM	NO ₂ ⁻ μM	NO ₃ ⁻ μM	SPM mg	C/N	PC %	PN %
Entire data	0.13	0.06	-0.65	-0.39	0.02	0.48	0.27	-0.31	0.53	0.12	-0.16
sp/su	-0.26	0.76 ⁺	-0.82 ⁺	-0.32	0.01	0.35	-0.40	-0.92*	0.15	0.18	0.31
Sal>1	-0.07	-0.14	-0.38	-0.43	-0.18	0.23	0.52	-0.19	0.46	-0.18	-0.38
Sal<1,	-0.21	0.29	-0.59	-0.39	0.26	0.76*	-0.11	-0.57	0.12	0.61	0.47
Sal>1, sp/su	-0.07	-0.70 ⁺	-0.41	-0.26	-0.42	0.03	0.05	-0.81 ⁺	-0.04	-0.10	0.14
Sal<1, sp/su	-0.48	0.72 ⁺	-0.80	-0.46	0.29	0.77 ⁺	-0.58	-0.87 ⁺	-0.17	0.69	0.67

260 4 Discussion

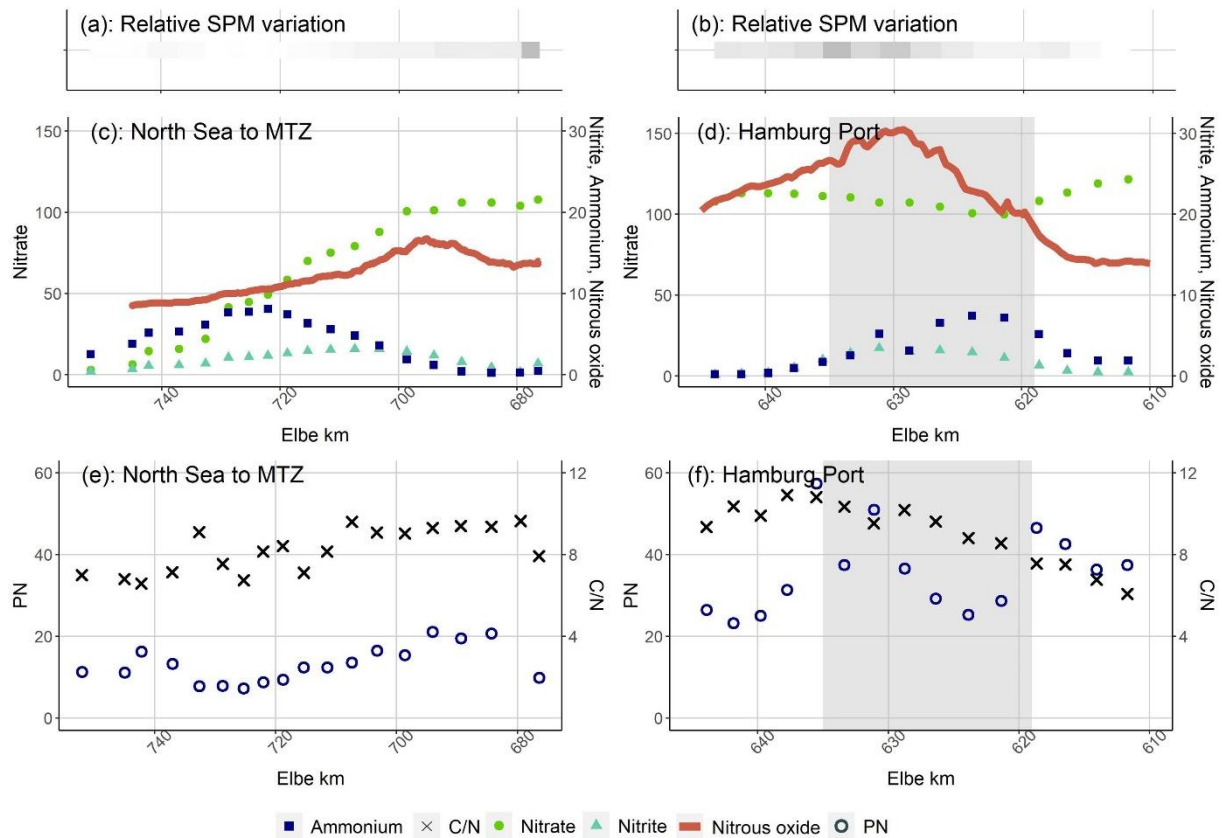
261 4.1 N₂O saturation and flux densities of the Elbe Estuary

262 The average N₂O saturation and flux density were 197 % and 39.9 ± 46.9 μmol m⁻² d⁻¹, respectively. The N₂O flux
 263 densities from the Elbe Estuary were in the mid-range of flux densities of other European estuaries ranging from
 264 2.9 μmol m⁻² d⁻¹ to 96.5 μmol m⁻² d⁻¹ (Garnier et al., 2006; Gonçalves et al., 2010; Murray et al., 2015) and average
 265 N₂O saturations fitted to values determined by Reading et al. (2020) for highly modified urban systems. The

266 relationship of N_2O_{xs} and AOU (Fig. 3), with changing slopes in the Port of Hamburg and mesohaline estuary, was
267 determined by either initial riverine N_2O production, or in-situ production along the estuary. During spring and
268 summer, we found increasing N_2O concentrations in the Hamburg Port region (see also Brase et al. (2017)), and
269 in the salinity gradient (stream kilometer 680 – 700, salinity ~5). Both N_2O peaks varied in magnitude and spatial
270 extension, suggesting in-situ biological production (Fig. 2g). This matches earlier research linking estuarine N_2O
271 fluxes to in-situ generation (e.g. Bange, 2006; Barnes and Upstill-Goddard, 2011; Murray et al., 2015).
272 Previous measurements of N_2O saturation and flux densities in the Elbe Estuary between the 1980s and 2015
273 (Hanke and Knauth, 1990; Barnes and Upstill-Goddard, 2011; Brase et al., 2017) showed a significant reduction
274 of N_2O saturation due to the reduced riverine nutrient load and higher dissolved oxygen concentrations (Brase et
275 al., 2017). However, since the BIOGEST study in 1997 (Barnes and Upstill-Goddard, 2011), N_2O remained
276 relatively stable at ~ 200 % saturation despite a concurrent decrease in TN concentration from ~400 $\mu\text{mol L}^{-1}$ to
277 around 200 $\mu\text{mol L}^{-1}$ (Fig. S2; Hanke and Knauth, 1990; Barnes and Upstill-Goddard, 2011; Brase et al., 2017;
278 Das Fachinformationssystem (FIS) der FGG Elbe, 2022). As N_2O saturation did not decrease in scale with riverine
279 nitrogen input, this suggests that in-situ N_2O production along the estuary is important. Dähnke et al. (2008)
280 showed a shift from dominating denitrification towards significant nitrification in the Elbe Estuary due to the
281 significant improvement of water quality after the reunification of Germany in 1990. In the following sections, we
282 investigate the biogeochemical controls of this in-situ production. For this purpose, we discuss the two zones of
283 intense N_2O production separately and also distinguish between cruises in spring and summer (water temperature
284 $> 10\text{ }^\circ\text{C}$) and in winter (water temperature $< 6\text{ }^\circ\text{C}$).

285 **4.2 N_2O production in spring and summer in the mesohaline estuary**

286 The N_2O peak in the transition between oligohaline and mesohaline estuary was accompanied by a sudden change
287 in the slope of the AOU vs N_2O_{xs} plots, (Fig. 3), pointing towards N_2O production in the oxic water column. Peaks
288 of nitrite and ammonium concentrations coincided with the elevated nitrous oxide saturations between Elbe km
289 680-700, with an ammonium peak around stream kilometer ~720, and a nitrite peak at ~700 (Fig. 4a). Highest
290 N_2O concentrations were usually measured between the nitrite peak and the region with highest turbidity (Fig. 4a,
291 September 2020, and Fig. S3-S13). This co-occurrence of nitrite accumulation and increased N_2O saturation has
292 been interpreted as signs for N_2O production via denitrification (e.g. Wertz et al., 2018; Sharma et al., 2022).
293 However, denitrification does not seem likely in this oxic water column. Such a succession of nitrite and
294 ammonium peaks is also typical for remineralization and nitrification, and the slight decrease of oxygen
295 concentrations around the higher N_2O saturation (Fig. 2g and i) suggests oxygen consumption, possibly caused by
296 these two processes. Sanders et al. (2018) measured small but detectable nitrification rates ($1 - 2\text{ } \mu\text{mol L}^{-1}\text{ d}^{-1}$) for
297 this region of the Elbe Estuary, suggesting that N_2O may be a side product of nitrification.



298

299 **Figure 4: Succession of N-bearing substances coming from the North Sea and in the Port of Hamburg in September**
 300 **2020: Relative change of SPM concentrations (a) from the North Sea and (b) in the Port of Hamburg. Nitrate in**
 301 **$\mu\text{mol L}^{-1}$, nitrite in $\mu\text{mol L}^{-1}$, ammonium in $\mu\text{mol L}^{-1}$ and nitrous oxide concentrations in nmol L^{-1} plotted against Elbe**
 302 **stream kilometers (c) from the North Sea and (d) in the Port of Hamburg. Particulate nitrogen concentrations in**
 303 **$\mu\text{mol L}^{-1}$ and C/N values plotted against stream kilometers (e) from the North Sea and (f) in the Port of Hamburg. The**
 304 **grey area in (f) and (f) shows the position of the Port of Hamburg.**

305 This suggests input of particulate matter from the North Sea and upstream particle transport towards the maximum
 306 turbidity zone of the estuary (MTZ). This transport mechanism is in line with Wolfstein and Kies (1999), who
 307 explained organic matter contents and chlorophyll a concentrations in the polyhaline part of the Elbe Estuary by
 308 input of freshly produced particulate matter of marine origin. Generally, maximum turbidity zones are generated
 309 by the balance between river-induced flushing and upstream transport of marine SPM, as a function of estuarine
 310 geomorphology, gravitational circulation and tidal flow, trapping the particles in the MTZ (Bianchi, 2007;
 311 Sommerfield and Wong, 2011; Winterwerp and Wang, 2013). Other studies detected N_2O production from water
 312 column nitrification in estuarine MTZs (e.g. Barnes and Owens, 1999; de Wilde and de Bie, 2000; Bange, 2006;
 313 Barnes and Upstill-Goddard, 2011; Harley et al., 2015), caused by high bacterial numbers, particulate nitrogen
 314 availability and long residence times (Murray et al., 2015).

315 For the selected dataset, we calculated a negative correlation between average SPM concentrations and N_2O
 316 saturation ($R = -0.81$, Table 5), and found that the N_2O peak was located downstream of the MTZ, and upstream
 317 of increasing nitrite and ammonium concentrations (Fig. 4a). This suggests that (1) the mere concentration of SPM
 318 is not the driving factor of nitrification as a source of N_2O , but that organic matter quality is key to biological
 319 turnover (Dähnke et al. 2022), and (2) the material transport from the North Sea upstream towards the MTZ
 320 (Kappenberg and Fanger, 2007; Schoer, 1990) is a main mechanism for N_2O generation. We find organic matter
 321 with low C/N ratios, and with relatively high PN and PC contents in the outermost samples (ranging from 5.9 in
 322 June 2020 to 8.8 August 2017), indicating fresh and easily degradable organic matter (Fig. S1, e.g. Redfield et al.

323 1963; Fraga et al. 1998; Middelburg and Herman 2007). Towards the MTZ, C/N values, PN and PC contents
324 decreased, indicating remineralization in the water column. This remineralization and subsequent nitrification can
325 then cause the observed succession of ammonium, nitrite and N₂O peaks (Fig. 4a), contributing to the high nitrate
326 concentrations in the MTZ, where high C/N values (9 – 11/16) indicate low organic matter quality (e.g. Hedges
327 and Keil 1995; Middelburg and Herman 2007). Overall, we conclude that remineralization of marine organic
328 matter, followed by nitrification, produced the N₂O peak in the salinity gradient of the Elbe Estuary. This
329 production was mainly fueled by fresh organic matter entering the estuary from the North Sea.

330 **4.3 Hamburg Port: N₂O production in spring and summer**

331 During all cruises, we measured highest N₂O saturation in the Port of Hamburg. These peaks can be caused by
332 input from a waste water treatment plant, by deepening and dredging operations, enhanced benthic production or
333 by in-situ production in the water column.

334 Point sources generally play a minor role in the Elbe Estuary (Hofmann et al., 2005; IKSE, 2018). We estimated
335 the wastewater discharge fraction of stream flow according to Büttner et al. (2020) for the waste water treatment
336 plant (WWTP) Köhlbrandhöft, which treats the waste water from the Hamburg metropolitan region, with less than
337 5 % even under low fresh water inflow. Thus, point sources seemed not to be the cause for the elevated N₂O
338 concentrations.

339 Dredging can be a potential source of N₂O in the water column. The estuary is continuously deepened and dredged
340 to grant access for large container ships, which stirs up bottom sediments. Ammonium concentrations in the
341 sediment pore water are high (Zander et al., 2020, 2022) and N₂O can be produced by nitrifier-denitrification in
342 the sediments (Deek et al., 2013). However, we found no correlation of high SPM concentrations and N₂O
343 saturation, indicating no major influence on N₂O dynamics from channel dredging and deepening.

344 Several studies identified the Hamburg Port region as a hotspot of biogeochemical turnover: Deek et al. (2013)
345 showed denitrification, where Sanders et al. (2018) measured intense nitrification.. Norbisch et al. (2022)
346 determined intense total alkalinity generation, and Dähnke et al. (2022) found that nitrogen turnover was driven
347 by high particulate organic matter in this region. Brase et al. (2017) identified the Hamburg port region as a hotspot
348 of N₂O production and hypothesized that simultaneous nitrification and sediment denitrification were responsible.
349 We use our expanded dataset to further evaluate this hypothesis and to identify drivers for N₂O production in the
350 port region.

351 During all cruises in spring and summer, we measured ammonium and nitrite peaks in the Hamburg Port region
352 (Fig. 2c and e, exemplary for September 2020 in Fig. 4b). Several researchers did address the nitrogen turnover
353 and this accumulation of nitrite and ammonium assuming that the sudden increase of water depth in the Port leads
354 to a light limitation and decomposition of riverine organic material (Schroeder, 1997; Schöl et al., 2014). This in
355 turn raises ammonium and nitrite concentrations and fosters nitrification in the port region (Sanders et al., 2018;
356 Dähnke et al., 2022).

357 High nitrite concentrations are favorable for N₂O production by nitrification and nitrifier-denitrification (Quick et
358 al., 2019), while low-oxygen conditions facilitate both nitrification and denitrification. We found that N₂O
359 saturation increased with decreasing discharge ($R = -0.48$, Table 5) during spring and summer. This further points
360 towards in-situ N₂O production, because denitrification and nitrification are more intense during longer residence
361 times (e.g. Nixon et al. 1996; Pind et al. 1997; Silvennoinen et al. 2007; Gonçalves et al. 2010). Overall, our data
362 showed the succession of ammonium, nitrite and N₂O production (Fig. 4b and supplementary material S3-S13)

363 confirming simultaneous sedimentary denitrification and nitrification in the water column responsible pathways
364 for N₂O production in the Port of Hamburg (Brase et al. 2017).

365 In spring and summer, we found no linear relationship between N₂O_{xs} and AOU in the Hamburg Port (Fig. 3). This
366 may result from combined N₂O production by nitrification and denitrification. However, oxygen saturation and
367 N₂O saturation were inversely correlated in Hamburg Port (Table 4 and 5), suggesting that N₂O production was
368 controlled by oxygen concentrations, and thus was related to oxygen consumption in the port region. Most (75 %)
369 of this oxygen consumption is caused by respiration whereas the remaining 25 % stem from nitrification (Schöl et
370 al., 2014; Sanders et al., 2018). This respiration in turn is determined by remineralization of algal material from
371 the upstream river that is transported to and respired within the port region (Schroeder, 1997; Kerner, 2000; Schöl
372 et al., 2014), linking estuarine N₂O production to river eutrophication. Fabisik et al. (2023) showed that algae could
373 additionally contribute to N₂O production. In the Elbe, fresh organic matter from the river with low C/N values as
374 well as high PN and PC contents entered the estuary. This organic material was rapidly degraded in the Hamburg
375 Port region (Fig. S1). Dähnke et al. (2022) found that labile organic matter fueled nitrification but also
376 denitrification in the fresh water part of the Elbe Estuary, which, as shown in our study, results in high N₂O
377 production in the Hamburg Port, leading to the reported negative correlations of PC and PN content with N₂O
378 saturation.

379 Overall, oxygen conditions mainly controlled N₂O production in the Hamburg Port region in spring and summer.
380 Since respiration of organic matter dominates oxygen drawdown in the port region, we deduce that N₂O production
381 there is linked to the decomposition of phytoplankton produced in the upstream Elbe River regions.

382 **4.4 Hamburg Port: N₂O production in winter**

383 In winter, low water temperature (< 6 °C) should hamper biological production (Koch et al., 1992; Halling-
384 Sorensen and Jorgensen, 1993). Indeed, we did not detect a N₂O peak in the MTZ in winter, but we find high N₂O
385 concentrations in the port region. For March 2022, we found a linear increase of N₂O_{xs} and AOU along with
386 oxygen consumption and increasing ammonium, nitrite and PN concentrations indicating nitrification in the
387 Hamburg Port producing N₂O. Unlike in summer, N₂O concentrations showed a flat increase extending far into
388 the oligohaline section of the estuary (Fig. 2, Fig. S1).

389 However, in March 2021, we found a sharp and sudden increase in N₂O, with a peak concentration that by far
390 exceeded internal biological sources in summer (Fig. 2h). An ammonium peak in the water column coincided with
391 the N₂O maximum (Fig. 2f and Fig. S11). If microbial activity is mostly temperature-inhibited, a local source of
392 N₂O in the port seems the most likely cause.

393 We considered intensified deepening operations in the Port of Hamburg one potential source of elevated N₂O
394 saturation. Deepening and dredging work occurred in the Hamburg Port region in 2021 (HPA, pers. Comm.,
395 Karrasch 2022), but, this also applied to 2022, when we saw no sharp N₂O peak (Fig. 2h). Furthermore, the regions
396 of deepening and dredging did not match the region of high N₂O concentrations, and turbidity at the time of
397 sampling did not change significantly compared to other cruises. Jointly, this suggests that channel dredging and
398 deepening was not the primary cause for the 2021 winter N₂O peak.

399 Another possible source of N₂O is the WWTP outflow in the Southern Elbe that joins the main estuary at stream
400 kilometer 626 (Fig. 1), matching the N₂O peak at stream kilometer 627 (Fig. 2h). As explained above (section 4.3),
401 the effect of this WWTP on N₂O saturations under normal conditions should be negligible. This peak can be the
402 result of an extraordinary event during our sampling. We indeed found that an extreme rain event occurred on

403 March 11th 2021 (HAMBURG WASSER, pers. Comm., Laurich 2022) with a statistical recurrence probability of
404 one to five years (<https://sri.hamburgwasser.de/>, last access: 04.04.2023). This rare event caused aggravated
405 operation conditions in the WWTP at the time of sampling. While the operators could still meet the limits for the
406 effluent levels of nitrate and ammonium, higher than usual ammonium loads exited the treatment plant at this time.
407 We assume that these elevated ammonium WWTP loads, were rapidly converted to N₂O as the warmer and
408 biologically active waste water entered the Elbe Estuary in March 2021. An important factor for aggravated
409 conditions was a temperature drop in the WWTP caused by cold rain water, we hypothesize that a similar rain
410 event in warmer months would not lead to comparable N₂O peaks.
411 Therefore, we argue that our March 2021 cruise likely represents an exception due to an extreme weather situation,
412 whereas normal winter conditions in the estuary comply with the N₂O production, like in March 2022.

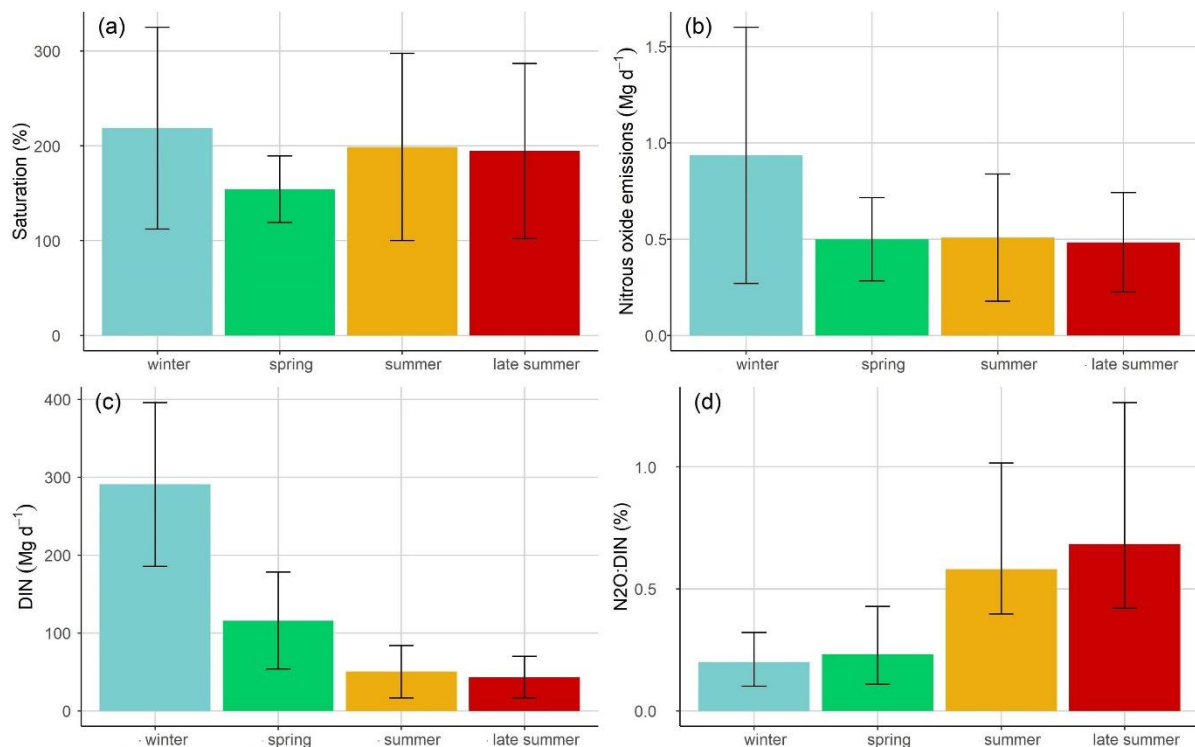
413 **4.5 Seasonally varying N₂O:DIN dynamic**

414 We calculated annual N₂O emissions of the Elbe Estuary ranging from 0.08 ± 0.03 Gg-N₂O yr⁻¹ to
415 0.25 ± 0.16 Gg-N₂O yr⁻¹, which varied from recent N₂O summer emission estimate of 0.18 ± 0.01 Gg-N₂O yr⁻¹ by
416 Brase et al. (2017). Estuarine N₂O emissions are affected by tides, diel variations and currents (Barnes et al., 2006;
417 Baulch et al., 2012; Gonçalves et al., 2015), all of which we did not address in our study. Range of possible
418 parametrizations of gas transfer coefficients further complicates a direct comparison of fluxes between studies
419 (Hall Jr. and Ulseth, 2020; Rosentreter et al., 2021), which were reflected in the big differences of our emission
420 estimates (Table 2). Therefore, a direct comparison to other studies is difficult.

421 In a more general approach, the relationship between N₂O and DIN (N₂O:DIN) is used for global estimates of N₂O
422 emissions (Kroeze et al., 2005, 2010; Ivens et al., 2011; Hu et al., 2016). Using publicly available data (Table S4
423 and S5), we calculated the amount of the annual nitrogen load released as N₂O. Depending on the parametrization
424 used for the gas transfer coefficients, 0.14 % to 0.67 % of the annual DIN loads of the Elbe Estuary were released
425 as N₂O (0.11 % to 0.57 % for TN loads). This is significantly less than the 1 % predicted by Kroeze et al. (2005),
426 but matches results from other estuaries with high agricultural input, e.g. Wells et al. (2018) with 0.3 % to 0.7 %
427 (0.1 % for TN loads) and Robinson et al. (1998) with 0.5 % (0.3 % for TN loads) as well as the 0.11 % to 0.37 %
428 estimated by Maavara et al. (2019), who used TN loads to predict global estuarine emissions.

429 At our site, highest emissions were estimated in winter (Fig. 5b) along with highest DIN loads (Fig. 5c). In spring,
430 summer and late summer, N₂O emissions reduced along with DIN loads (Fig. 5b, c). However, N₂O release did
431 not scale with the seasonal change of DIN. In winter, 0.10 % to 0.32 % of DIN were released as N₂O, whereas
432 during the other seasons, up to 1.26 % were emitted. Thus, our results corroborate that there is a deviating
433 relationship between DIN and N₂O (Borges et al., 2015; Marzadri et al., 2017; Wells et al., 2018) showing that
434 this relationship even varies seasonally on site due to changing drivers for N₂O production and emissions.

435 Next to DIN loads, we find that organic matter is an important driver for N₂O production by providing substrate
436 for nitrification. Furthermore, the comparison of our results with previous measurements in the Elbe Estuary
437 revealed that N₂O saturation stopped to scale with DIN input after the 1990s (section 4.1). The significant regime
438 change after the 1990s enabled phytoplankton growth to reestablish in the river (Kerner, 2000; Amann et al., 2012;
439 Hillebrand et al., 2018; Rewrie et al., submitted) and led to high nitrification rates in the estuary (Dähnke et al.,
440 2008; Sanders et al., 2018), supporting the overarching control of organic matter on N₂O production and emissions
441 along the Elbe Estuary.



442
 443 **Figure 5: (a) Average nitrous oxide saturation for each season, (b) average nitrous oxide emissions for each season**
 444 **calculated after Borges et al. (2004), (c) average DIN loads for each season and (d) ratio of nitrous oxide emissions and**
 445 **DIN loads (N₂O:DIN) for each season. The error bars represent the standard deviations for (a), (b) and (c). The**
 446 **N₂O:DIN ratios is shown as average values calculated for each parametrization and wind speeds with error bars**
 447 **representing their variability.**

449 5 Conclusions

450 Overall, the Elbe is a year-round source of N₂O to the atmosphere, with highest emission occurring in winter,
 451 along with high DIN loads and high wind speeds. However, summer N₂O saturation and emissions did not decrease
 452 with lower riverine nitrogen input suggesting variable relations of DIN and N₂O (Borges et al., 2004; Marzadri et
 453 al., 2017; Wells et al., 2018), and seasonal variability of this ratio caused by changing drivers for N₂O production
 454 and emissions. Two hot-spots of N₂O production were found in the Elbe Estuary: the Port of Hamburg and the
 455 mesohaline estuary near the estuarine turbidity maximum. Biological N₂O production was enhanced by warmer
 456 temperatures and fueled by riverine organic matter in the Hamburg Port or marine organic matter in the MTZ. A
 457 comparison with historical N₂O measurements in the Elbe Estuary revealed that N₂O saturation did not decrease
 458 with DIN input after the 1990s. The improvement of water quality in the Elbe Estuary allowed phytoplankton
 459 growth after the reunification of Germany in 1990s (Kerner, 2000; Amann et al., 2012; Hillebrand et al., 2018;
 460 Rewrie et al., submitted) and led to a switch from dominant denitrification to high nitrification (Dähnke et al.,
 461 2008; Sanders et al., 2018), supporting the overarching control of organic matter on N₂O production along the
 462 Elbe Estuary. Thus, our findings indicate that DIN availability is not the sole control of N₂O production in estuaries
 463 with high agricultural input. High organic matter availability due to phytoplankton blooms driven by river
 464 eutrophication fuels nitrification and subsequent N₂O emissions, causing a decoupling of the N₂O:DIN ratio.
 465 Therefore, N₂O emissions in heavily managed estuaries with high agricultural loads are clearly linked to
 466 eutrophication. Consequently, reducing nitrogen input alone is not sufficient to minimize N₂O emissions from
 467 estuaries. Further measures are needed to prevent the developments of intense phytoplankton blooms in rivers and

468 estuaries. Especially considering climate change projections of more frequent and extensive draughts and warmer
469 temperatures (IPCC, 2022), which potentially fuel phytoplankton growth (e.g. Scharfe et al., 2009; Kamjunke et
470 al., 2021; IPCC, 2022).

471 **Data availability**

472 The dataset generated and/or analyzed in this study are currently available upon request from the corresponding
473 author and will be made publicly available under coastMap Geoportal (www.coastmap.org) connecting to
474 PANGAEA. (<https://www.pangaea.de/>) with DOI availability in the near future.

475 **Authors contribution**

476 GS, TS and KD designed this study. GS did the sampling and measurements for cruises from 2020 to 2022 as well
477 as the data interpretation and evaluation. TS was responsible for the sampling and measurements for cruises done
478 in 2017 and 2019. YGV provided the oxygen data correction from the FerryBox data. KD, HWB, YGV and TS
479 contributed with scientific and editorial recommendations. GS prepared the manuscript with contributions of all
480 co-authors.

481 **Competing interest**

482 The authors declare that they have no conflict of interest.

483 **Acknowledgments**

484 This study was funded by the Deutsche Forschungsgemeinschaft (DFG, German Research Foundation) under
485 Germany's Excellence Strategy – EXC 2037 “CLICCS - Climate, Climatic Change, and Society” – Project
486 Number: 390683824, contribution to the Center for Earth System Research and Sustainability (CEN) of Universität
487 Hamburg. Parts of the study were done in the framework of the cross-topic activity MOSES (Modular Observation
488 Solutions for Earth Systems) within the Helmholtz program Changing Earth (Topic 4.1). We thank the crew of
489 R/V Ludwig Prandtl for the great support during the cruises. Thanks to Leon Schmidt and the entire working group
490 “Aquatic nutrients cycles” for measuring nutrients and the support during the campaigns. We are thankful for the
491 Hereon FerryBox Team for providing the FerryBox data. Thanks to the working group of Biogeochemistry at the
492 Institute for Geology of the University Hamburg for measuring C/N ratios, PC and PN fractions. We thank Frank
493 Laurich (HAMBURG WASSER) and Dr. Maja Karrasch (Hamburg Port Authority) for their interest in our N₂O
494 measurements and their willingness to provide information. Thanks to Victoria Oritz (Federal Waterways and
495 Engineering and Research Institute) for providing the respective areas of the Elbe Estuary. Thanks to the NOAA
496 ESRL GML CCGG Group for providing high quality, readily accessible atmospheric N₂O data.

497 **References**

498 Amann, T., Weiss, A., and Hartmann, J.: Carbon dynamics in the freshwater part of the Elbe estuary, Germany:
499 Implications of improving water quality, *Estuar. Coast. Shelf Sci.*, 107, 112–121,
500 <https://doi.org/10.1016/j.ecss.2012.05.012>, 2012.

- 501 Bange, H. W.: Nitrous oxide and methane in European coastal waters, *Estuar. Coast. Shelf Sci.*, 70, 361–374,
502 <https://doi.org/10.1016/j.ecss.2006.05.042>, 2006.
- 503 Bange, H. W.: Chapter 2 - Gaseous Nitrogen Compounds (NO, N₂O, N₂, NH₃) in the Ocean, *Nitrogen Mar.*
504 *Environ. Second Ed.*, 51–94, <https://doi.org/10.1016/B978-0-12-372522-6.00002-5>, 2008.
- 505 Barnes, J. and Owens, N. J. P.: Denitrification and Nitrous Oxide Concentrations in the Humber Estuary, UK, and
506 Adjacent Coastal Zones, *Mar. Pollut. Bull.*, 37, 247–260, [https://doi.org/10.1016/S0025-326X\(99\)00079-X](https://doi.org/10.1016/S0025-326X(99)00079-X), 1999.
- 507 Barnes, J. and Upstill-Goddard, R. C.: N₂O seasonal distributions and air-sea exchange in UK estuaries:
508 Implications for the tropospheric N₂O source from European coastal waters, *J. Geophys. Res. Biogeosciences*,
509 116, <https://doi.org/10.1029/2009JG001156>, 2011.
- 510 Barnes, J., Ramesh, R., Purvaja, R., Nirmal Rajkumar, A., Senthil Kumar, B., Krithika, K., Ravichandran, K.,
511 Uher, G., and Upstill-Goddard, R.: Tidal dynamics and rainfall control N₂O and CH₄ emissions from a pristine
512 mangrove creek, *Geophys. Res. Lett.*, 33, <https://doi.org/10.1029/2006GL026829>, 2006.
- 513 Baulch, H. M., Dillon, P. J., Maranger, R., Venkiteswaran, J. J., Wilson, H. F., and Schiff, S. L.: Night and day:
514 short-term variation in nitrogen chemistry and nitrous oxide emissions from streams, *Freshw. Biol.*, 57, 509–525,
515 <https://doi.org/10.1111/j.1365-2427.2011.02720.x>, 2012.
- 516 BAW, Oritz, V.: pers. Comm.: Flächen des Elbe Ästuars, 2023.
- 517 Beaulieu, J. J., Shuster, W. D., and Rebolz, J. A.: Nitrous Oxide Emissions from a Large, Impounded River: The
518 Ohio River, *Environ. Sci. Technol.*, 44, 7527–7533, <https://doi.org/10.1021/es1016735>, 2010.
- 519 Bergemann, M.: Die Trübungszone in der Tideelbe - Beschreibung der räumlichen und zeitlichen Entwicklung,
520 Wassergütestelle Elbe, 2004.
- 521 Bergemann, M. and Gaumert, T.: Elbebericht 2008: Ergebnisse des nationalen Überwachungsprogramms Elbe der
522 Bundesländer über den ökologischen und chemischen Zustand der Elbe nach EG-WRRL sowie der
523 Trendentwicklung von Stoffen und Schadstoffgruppen, Flussgebietsgemeinschaft Elbe (FGG Elbe), Hamburg,
524 2008.
- 525 van Beusekom, J. E. E., Carstensen, J., Dolch, T., Grage, A., Hofmeister, R., Lenhart, H., Kerimoglu, O., Kolbe,
526 K., Pätsch, J., Rick, J., Rönn, L., and Ruiter, H.: Wadden Sea Eutrophication: Long-Term Trends and Regional
527 Differences, *Front. Mar. Sci.*, 6, 370, <https://doi.org/10.3389/fmars.2019.00370>, 2019.
- 528 Bianchi, T. S.: *Biogeochemistry of Estuaries*, Oxford University Press, New York, 706 pp., 2007.
- 529 Boehlich, M. J. and Strotmann, T.: The Elbe Estuary, *Küste*, 74, 288–306, 2008.
- 530 Boehlich, M. J. and Strotmann, T.: Das Elbeästuar, *Küste*, 87, Kuratorium für Forschung im Küsteningenieurwesen
531 (KFKI), <https://doi.org/10.18171/1.087106>, 2019.
- 532 Borges, A., Vanderborght, J.-P., Schiettecatte, L.-S., Gazeau, F., Ferrón-Smith, S., Delille, B., and Frankignoulle,
533 M.: Variability of gas transfer velocity of CO₂ in a macrotidal estuary (The Scheldt), *Estuaries*, 27, 593–603,
534 <https://doi.org/10.1007/BF02907647>, 2004.
- 535 Borges, A. V., Darchambeau, F., Teodoru, C. R., Marwick, T. R., Tamooh, F., Geeraert, N., Omengo, F. O.,
536 Guérin, F., Lambert, T., Morana, C., Okuku, E., and Bouillon, S.: Globally significant greenhouse-gas emissions
537 from African inland waters, *Nat. Geosci.*, 8, 637–642, <https://doi.org/10.1038/ngeo2486>, 2015.
- 538 Bouwman, A. F., Bierkens, M. F. P., Griffioen, J., Hefting, M. M., Middelburg, J. J., Middelkoop, H., and Slomp,
539 C. P.: Nutrient dynamics, transfer and retention along the aquatic continuum from land to ocean: towards
540 integration of ecological and biogeochemical models, *Biogeosciences*, 10, 1–23, [https://doi.org/10.5194/bg-10-1-](https://doi.org/10.5194/bg-10-1-2013)
541 2013, 2013.
- 542 Brase, L., Bange, H. W., Lendt, R., Sanders, T., and Dähnke, K.: High Resolution Measurements of Nitrous Oxide
543 (N₂O) in the Elbe Estuary, *Front. Mar. Sci.*, 4, 162, <https://doi.org/10.3389/fmars.2017.00162>, 2017.

- 544 Büttner, O., Jawitz, J. W., and Borchardt, D.: Ecological status of river networks: stream order-dependent impacts
545 of agricultural and urban pressures across ecoregions, *Environ. Res. Lett.*, 15, 1040b3,
546 <https://doi.org/10.1088/1748-9326/abb62e>, 2020.
- 547 Clark, J. F., Schlosser, P., Simpson, H. J., Stute, M., Wanninkhof, R., and Ho, D. T.: Relationship between gas
548 transfer velocities and wind speeds in the tidal Hudson River determined by the dual tracer technique, in: *Air-
549 Water Gas Transfer*, edited by: Jähne, B. and Monahan, E. C., AEON Verlag, Hanau, 785–800, 1995.
- 550 Crossland, C. J., Baird, D., Ducrotoy, J.-P., Lindeboom, H., Buddemeier, R. W., Dennison, W. C., Maxwell, B.
551 A., Smith, S. V., and Swaney, D. P.: The Coastal Zone — a Domain of Global Interactions, in: *Coastal Fluxes in
552 the Anthropocene: The Land-Ocean Interactions in the Coastal Zone Project of the International Geosphere-
553 Biosphere Programme*, edited by: Crossland, C. J., Kremer, H. H., Lindeboom, H. J., Marshall Crossland, J. I., and
554 Le Tissier, M. D. A., Springer, Berlin, Heidelberg, 1–37, https://doi.org/10.1007/3-540-27851-6_1, 2005.
- 555 Dähnke, K., Bahlmann, E., and Emeis, K.-C.: A nitrate sink in estuaries? An assessment by means of stable nitrate
556 isotopes in the Elbe estuary, *Limnol. Oceanogr.*, 53, 1504–1511, <https://doi.org/10.4319/lo.2008.53.4.1504>, 2008.
- 557 Dähnke, K., Sanders, T., Voynova, Y., and Wankel, S. D.: Nitrogen isotopes reveal a particulate-matter-driven
558 biogeochemical reactor in a temperate estuary, *Biogeosciences*, 19, 5879–5891, <https://doi.org/10.5194/bg-19-5879-2022>, 2022.
- 560 Deek, A., Dähnke, K., van Beusekom, J., Meyer, S., Voss, M., and Emeis, K.-C.: N₂ fluxes in sediments of the
561 Elbe Estuary and adjacent coastal zones, *Mar. Ecol. Prog. Ser.*, 493, 9–21, <https://doi.org/10.3354/meps10514>,
562 2013.
- 563 Dlugokencky, E. J., Crotwell, A. M., Mund, J. W., Crotwell, M. J., and Thoning, K. W.: Earth System Research
564 Laboratory Carbon Cycle and Greenhouse Gases Group Flask-Air Sample Measurements of N₂O at Global and
565 Regional Background Sites, 1967-Present [Data set], <https://doi.org/10.15138/53G1-X417>, 2022.
- 566 Fabisik, F., Guieysse, B., Procter, J., and Plouviez, M.: Nitrous oxide (N₂O) synthesis by the freshwater
567 cyanobacterium *Microcystis aeruginosa*, *Biogeosciences*, 20, 687–693, <https://doi.org/10.5194/bg-20-687-2023>,
568 2023.
- 569 FGG Elbe: Nährstoffminderungsstrategie für die Flussgebietsgemeinschaft Elbe, Flussgebietsgemeinschaft Elbe
570 (FGG Elbe), Magdeburg, 2018.
- 571 Das Fachinformationssystem (FIS) der FGG Elbe: [https://www.elbe-
572 datenportal.de/FisFggElbe/content/start/ZurStartseite.action;jsessionid=A37EDCF5B5EC1ECB15091447E64EC
573 538](https://www.elbe-datenportal.de/FisFggElbe/content/start/ZurStartseite.action;jsessionid=A37EDCF5B5EC1ECB15091447E64EC538), last access: 21 November 2022.
- 574 Fraga, F., Ríos, A. F., Pérez, F. F., and Figueiras, F. G.: Theoretical limits of oxygen:carbon and oxygen:nitrogen
575 ratios during photosynthesis and mineralisation of organic matter in the sea, *Sci. Mar.*, 62, 161–168,
576 <https://doi.org/10.3989/scimar.1998.62n1-2161>, 1998.
- 577 Garnier, J., Cébron, A., Tallec, G., Billen, G., Sebilo, M., and Martinez, A.: Nitrogen Behaviour and Nitrous Oxide
578 Emission in the Tidal Seine River Estuary (France) as Influenced by Human Activities in the Upstream Watershed,
579 *Biogeochemistry*, 77, 305–326, <https://doi.org/10.1007/s10533-005-0544-4>, 2006.
- 580 Gaumert, T. and Bergemann, M.: Sauerstoffgehalt der Tideelbe - Entwicklung der kritischen Sauerstoffgehalte im
581 Jahr 2007 und in den Vorjahren, Erörterung möglicher Ursachen und Handlungsoptionen,
582 Flussgebietsgemeinschaft Elbe, 2007.
- 583 Geerts, L., Wolfstein, K., Jacobs, S., van Damme, S., and Vandenbruwaene, W.: Zonation of the TIDE estuaries,
584 TIDE toolbox, 2012.
- 585 Gonçalves, C., Brogueira, M. J., and Camões, M. F.: Seasonal and tidal influence on the variability of nitrous oxide
586 in the Tagus estuary, Portugal, *Sci. Mar.*, 74, 57–66, <https://doi.org/10.3989/scimar.2010.74s1057>, 2010.
- 587 Gonçalves, C., Brogueira, M. J., and Nogueira, M.: Tidal and spatial variability of nitrous oxide (N₂O) in Sado
588 estuary (Portugal), *Estuar. Coast. Shelf Sci.*, 167, 466–474, <https://doi.org/10.1016/j.ecss.2015.10.028>, 2015.

- 589 Hall Jr., R. O. and Ulseth, A. J.: Gas exchange in streams and rivers, *WIREs Water*, 7, e1391,
590 <https://doi.org/10.1002/wat2.1391>, 2020.
- 591 Halling-Sorensen, B. and Jorgensen, S. E. (Eds.): 3. Process Chemistry and Biochemistry of Nitrification, in:
592 *Studies in Environmental Science*, vol. 54, Elsevier, 55–118, [https://doi.org/10.1016/S0166-1116\(08\)70525-9](https://doi.org/10.1016/S0166-1116(08)70525-9),
593 1993.
- 594 HAMBURG WASSER, Laurich, F.: pers. Comm.: N₂O in der Elbe, 2022.
- 595 Hanke, V.-R. and Knauth, H.-D.: N₂O-Gehalte in Wasser-und Luftproben aus den Bereichen der Tideelbe und der
596 Deutschen Bucht, GKSS-Forschungszentrum, Weinheim, 1990.
- 597 Hansen, H. P. and Koroleff, F.: Determination of nutrients, in: *Methods of Seawater Analysis*, John Wiley & Sons,
598 Ltd, 159–228, <https://doi.org/10.1002/9783527613984.ch10>, 1999.
- 599 Harley, J. F., Carvalho, L., Dudley, B., Heal, K. V., Rees, R. M., and Skiba, U.: Spatial and seasonal fluxes of the
600 greenhouse gases N₂O, CO₂ and CH₄ in a UK macrotidal estuary, *Estuar. Coast. Shelf Sci.*, 153, 62–73,
601 <https://doi.org/10.1016/j.ecss.2014.12.004>, 2015.
- 602 Hedges, J. I. and Keil, R. G.: Sedimentary organic matter preservation: an assessment and speculative synthesis,
603 *Mar. Chem.*, 49, 81–115, [https://doi.org/10.1016/0304-4203\(95\)00008-F](https://doi.org/10.1016/0304-4203(95)00008-F), 1995.
- 604 Hein, S. S. V., Sohr, V., Nehlsen, E., Strotmann, T., and Fröhle, P.: Tidal Oscillation and Resonance in Semi-
605 Closed Estuaries—Empirical Analyses from the Elbe Estuary, *North Sea, Water*, 13, 848,
606 <https://doi.org/10.3390/w13060848>, 2021.
- 607 Schleswig-Holstein u. Hamburg: Mittlere Windgeschwindigkeit (1986-2015)* | Norddeutscher Klimamonitor:
608 [https://www.norddeutscher-klimamonitor.de/klima/1986-2015/jahr/mittlere-windgeschwindigkeit/schleswig-](https://www.norddeutscher-klimamonitor.de/klima/1986-2015/jahr/mittlere-windgeschwindigkeit/schleswig-holstein-hamburg/coastdat-1.html)
609 [holstein-hamburg/coastdat-1.html](https://www.norddeutscher-klimamonitor.de/klima/1986-2015/jahr/mittlere-windgeschwindigkeit/schleswig-holstein-hamburg/coastdat-1.html), last access: 27 April 2023.
- 610 Hillebrand, G., Hardenbicker, P., Fischer, H., Otto, W., and Vollmer, S.: Dynamics of total suspended matter and
611 phytoplankton loads in the river Elbe, *J. Soils Sediments*, 18, 3104–3113, [https://doi.org/10.1007/s11368-018-](https://doi.org/10.1007/s11368-018-1943-1)
612 [1943-1](https://doi.org/10.1007/s11368-018-1943-1), 2018.
- 613 Hofmann, J., Behrendt, H., Gilbert, A., Janssen, R., Kannen, A., Kappenberg, J., Lenhart, H., Lise, W., Nunneri,
614 C., and Windhorst, W.: Catchment–coastal zone interaction based upon scenario and model analysis: Elbe and the
615 German Bight case study, *Reg. Environ. Change*, 5, 54–81, <https://doi.org/10.1007/s10113-004-0082-y>, 2005.
- 616 HPA and Freie und Hansestadt Hamburg: *Deutsches Gewässerkundliches Jahrbuch - Elbegebiet, Teil III, Untere*
617 *Elbe ab der Havelmündung - 2014*, Hamburg, 2017.
- 618 HPA, Karrasch, M.: pers. Comm.: Anfrage wegen N₂O Peak - Baggerarbeiten Elbe März 2021 und März 2022,
619 2022.
- 620 Hu, M., Chen, D., and Dahlgren, R. A.: Modeling nitrous oxide emission from rivers: a global assessment, *Glob.*
621 *Change Biol.*, 22, 3566–3582, <https://doi.org/10.1111/gcb.13351>, 2016.
- 622 IKSE: Strategie zur Minderung der Nährstoffeinträge in Gewässer in der internationalen Flussgebietsgemeinschaft
623 Elbe, Internationale Kommission zur Schutz der Elbe, Magdeburg, 2018.
- 624 IPCC: *Climate Change 2021: The Physical Science Basis. Contribution of Working Group I to the Sixth*
625 *Assessment Report of the Intergovernmental Panel on Climate Change*, edited by: Masson-Delmotte, V., Zhai, P.,
626 Pirani, A., Connors, S. L., Péan, C., Berger, S., Caud, N., Chen, Y., Goldfarb, L., Gomis, M. I., Huang, M., Leitzell,
627 K., Lonnoy, E., Matthews, J. B. R., Maycock, T. K., Waterfield, T., Yelekçi, Ö., Yu, R., and Zhou, B., Cambridge
628 University Press, Cambridge, United Kingdom and New York, NY, USA,
629 <https://doi.org/10.1017/9781009157896>, 2021.
- 630 IPCC: *Climate Change 2022: Impacts, Adaptation and Vulnerability. Contribution of Working Group II to the*
631 *Sixth Assessment Report of the Intergovernmental Panel on Climate Change.*, edited by: Pörtner, H.-O., Roberts,
632 D. C., Tignor, M. M. B., Poloczanska, E. S., Mintenbeck, K., Alegría, A., Craig, M., Langsdorf, S., Lösschke, S.,

- 633 Möller, V., Okem, A., and Rama, B., Cambridge University Press, Cambridge, UK and New York, NY, USA,
634 3056 pp., <https://doi.org/10.1017/9781009325844>, 2022.
- 635 Ivens, W. P. M. F., Tysmans, D. J. J., Kroeze, C., Löhr, A. J., and van Wijnen, J.: Modeling global N₂O emissions
636 from aquatic systems, *Curr. Opin. Environ. Sustain.*, 3, 350–358, <https://doi.org/10.1016/j.cosust.2011.07.007>,
637 2011.
- 638 Ji, Q., Frey, C., Sun, X., Jackson, M., Lee, Y.-S., Jayakumar, A., Cornwell, J. C., and Ward, B. B.: Nitrogen and
639 oxygen availabilities control water column nitrous oxide production during seasonal anoxia in the Chesapeake
640 Bay, *Biogeosciences*, 15, 6127–6138, <https://doi.org/10.5194/bg-15-6127-2018>, 2018.
- 641 Johannsen, A., Dähnke, K., and Emeis, K.: Isotopic composition of nitrate in five German rivers discharging into
642 the North Sea, *Org. Geochem.*, 39, 1678–1689, <https://doi.org/10.1016/j.orggeochem.2008.03.004>, 2008.
- 643 Kamjunke, N., Rode, M., Baborowski, M., Kunz, J., Zehner, J., Borchardt, D., and Weitere, M.: High irradiation
644 and low discharge promote the dominant role of phytoplankton in riverine nutrient dynamics, *Limnol. Oceanogr.*,
645 66, <https://doi.org/10.1002/lno.11778>, 2021.
- 646 Kappenberg, J. and Fanger, H.-U.: Sedimenttransportgeschehen in der tidebeeinflussten Elbe, der Deutschen Bucht
647 und in der Nordsee, GKSS-Forschungszentrum, Geesthacht, 2007.
- 648 Kassambara, A.: ggpubr: “ggplot2” Based Publication Ready Plots, 2023.
- 649 Kerner, M.: Interactions between local oxygen deficiencies and heterotrophic microbial processes in the elbe
650 estuary, *Limnologica*, 30, 137–143, [https://doi.org/10.1016/S0075-9511\(00\)80008-0](https://doi.org/10.1016/S0075-9511(00)80008-0), 2000.
- 651 Knowles, R.: Denitrification, *Microbiol. Rev.*, 46, 43–70, <https://doi.org/10.1128/mr.46.1.43-70.1982>, 1982.
- 652 Koch, M. S., Maltby, E., Oliver, G. A., and Bakker, S. A.: Factors controlling denitrification rates of tidal mudflats
653 and fringing salt marshes in south-west England, *Estuar. Coast. Shelf Sci.*, 34, 471–485,
654 [https://doi.org/10.1016/S0272-7714\(05\)80118-0](https://doi.org/10.1016/S0272-7714(05)80118-0), 1992.
- 655 Kroeze, C., Dumont, E., and Seitzinger, S. P.: New estimates of global emissions of N₂O from rivers and estuaries,
656 *Environ. Sci.*, 2, 159–165, <https://doi.org/10.1080/15693430500384671>, 2005.
- 657 Kroeze, C., Dumont, E., and Seitzinger, S.: Future trends in emissions of N₂O from rivers and estuaries, *J. Integr.*
658 *Environ. Sci.*, 7, 71–78, <https://doi.org/10.1080/1943815X.2010.496789>, 2010.
- 659 Maavara, T., Lauerwald, R., Laruelle, G. G., Akbarzadeh, Z., Bouskill, N. J., Van Cappellen, P., and Regnier, P.:
660 Nitrous oxide emissions from inland waters: Are IPCC estimates too high?, *Glob. Change Biol.*, 25, 473–488,
661 <https://doi.org/10.1111/gcb.14504>, 2019.
- 662 Marzadri, A., Dee, M. M., Tonina, D., Bellin, A., and Tank, J. L.: Role of surface and subsurface processes in
663 scaling N₂O emissions along riverine networks, *Proc. Natl. Acad. Sci.*, 114, 4330–4335,
664 <https://doi.org/10.1073/pnas.1617454114>, 2017.
- 665 Middelburg, J. J. and Herman, P. M. J.: Organic matter processing in tidal estuaries, *Mar. Chem.*, 106, 127–147,
666 <https://doi.org/10.1016/j.marchem.2006.02.007>, 2007.
- 667 Middelburg, J. J. and Nieuwenhuize, J.: Uptake of dissolved inorganic nitrogen in turbid, tidal estuaries, *Mar.*
668 *Ecol.-Prog. Ser.*, 192, 79–88, <https://doi.org/10.3354/meps192079>, 2000.
- 669 Murray, R. H., Erler, D. V., and Eyre, B. D.: Nitrous oxide fluxes in estuarine environments: response to global
670 change, *Glob. Change Biol.*, 21, 3219–3245, <https://doi.org/10.1111/gcb.12923>, 2015.
- 671 Nevison, C., Butler, J. H., and Elkins, J. W.: Global distribution of N₂O and the Δ N₂O-AOU yield in the
672 subsurface ocean, *Glob. Biogeochem. Cycles*, 17, 1119, <https://doi.org/10.1029/2003GB002068>, 2003.
- 673 Nightingale, P. D., Malin, G., Law, C. S., Watson, A. J., Liss, P. S., Liddicoat, M. I., Boutin, J., and Upstill-
674 Goddard, R. C.: In situ evaluation of air-sea gas exchange parameterizations using novel conservative and volatile
675 tracers, *Glob. Biogeochem. Cycles*, 14, 373–387, <https://doi.org/10.1029/1999GB900091>, 2000.

676 Nixon, S. W., Ammerman, J. W., Atkinson, L. P., Berounsky, V. M., Billen, G., Boicourt, W. C., Boynton, W. R.,
677 Church, T. M., Ditoro, D. M., Elmgren, R., Garber, J. H., Giblin, A. E., Jahnke, R. A., Owens, N. J. P., Pilson, M.
678 E. Q., and Seitzinger, S. P.: The fate of nitrogen and phosphorus at the land-sea margin of the North Atlantic
679 Ocean, *Biogeochemistry*, 35, 141–180, <https://doi.org/10.1007/BF02179826>, 1996.

680 Norbirsath, M., Pätsch, J., Dähnke, K., Sanders, T., Schulz, G., van Beusekom, J. E. E., and Thomas, H.: Metabolic
681 alkalinity release from large port facilities (Hamburg, Germany) and impact on coastal carbon storage,
682 *Biogeosciences*, 19, 5151–5165, <https://doi.org/10.5194/bg-19-5151-2022>, 2022.

683 Pätsch, J., Serna, A., Dähnke, K., Schlarbaum, T., Johannsen, A., and Emeis, K.-C.: Nitrogen cycling in the
684 German Bight (SE North Sea) — Clues from modelling stable nitrogen isotopes, *Cont. Shelf Res.*, 30, 203–213,
685 <https://doi.org/10.1016/j.csr.2009.11.003>, 2010.

686 Pind, A., Risgaard-Petersen, N., and Revsbech, N. P.: Denitrification and microphytobenthic NO₃- consumption
687 in a Danish lowland stream: diurnal and seasonal variation, *Aquat. Microb. Ecol.*, 12, 275–284,
688 <https://doi.org/10.3354/ame012275>, 1997.

689 Quick, A. M., Reeder, W. J., Farrell, T. B., Tonina, D., Feris, K. P., and Benner, S. G.: Nitrous oxide from streams
690 and rivers: A review of primary biogeochemical pathways and environmental variables, *Earth-Sci. Rev.*, 191, 224–
691 262, <https://doi.org/10.1016/j.earscirev.2019.02.021>, 2019.

692 Quiel, K., Becker, A., Kirchesch, V., Schöl, A., and Fischer, H.: Influence of global change on phytoplankton and
693 nutrient cycling in the Elbe River, *Reg. Environ. Change*, 11, 405–421, [https://doi.org/10.1007/s10113-010-0152-](https://doi.org/10.1007/s10113-010-0152-2)
694 2, 2011.

695 The R Stats Package, Version 4.0.2:
696 <https://www.rdocumentation.org/packages/stats/versions/3.6.2/topics/prcomp>, last access: 29 January 2021.

697 Radach, G. and Pätsch, J.: Variability of continental riverine freshwater and nutrient inputs into the North Sea for
698 the years 1977–2000 and its consequences for the assessment of eutrophication, *Estuaries Coasts*, 30, 66–81,
699 <https://doi.org/10.1007/BF02782968>, 2007.

700 Reading, M. J., Tait, D. R., Maher, D. T., Jeffrey, L. C., Looman, A., Holloway, C., Shishaye, H. A., Barron, S.,
701 and Santos, I. R.: Land use drives nitrous oxide dynamics in estuaries on regional and global scales, *Limnol.*
702 *Oceanogr.*, 65, 1903–1920, <https://doi.org/10.1002/lno.11426>, 2020.

703 Redfield, A. C., Ketchum, B. H., and Richards, F. A.: The influence of organisms on the composition of sea-water,
704 *Compos. Seawater Comp. Descr. Oceanogr. Sea Ideas Obs. Prog. Study Seas*, 2, 26–77, 1963.

705 Rewrie, L. C. V., Voynova, Y. G., van Beusekom, J. E. E., Sanders, T., Körtzinger, A., Brix, H., Ollesch, G., and
706 Baschek, B.: Significant shifts in inorganic carbon and ecosystem state in a temperate estuary (1985 - 2018),
707 *Limnol. Oceanogr.*, submitted.

708 Rhee, T. S.: The process of air -water gas exchange and its application, Texas A&M University, College Station,
709 2000.

710 Rhee, T. S., Kettle, A. J., and Andreae, M. O.: Methane and nitrous oxide emissions from the ocean: A
711 reassessment using basin-wide observations in the Atlantic, *J. Geophys. Res. Atmospheres*, 114, D12304,
712 <https://doi.org/10.1029/2008JD011662>, 2009.

713 Robinson, A. D., Nedwell, D. B., Harrison, R. M., and Ogilvie, B. G.: Hypernutrified estuaries as sources of N₂
714 O emission to the atmosphere: the estuary of the River Colne, Essex, UK, *Mar. Ecol. Prog. Ser.*, 164, 59–71,
715 <https://doi.org/10.3354/meps164059>, 1998.

716 Rosenhagen, G., Schatzmann, M., and Schrön, A.: Das Klima der Metropolregion auf Grundlage meteorologischer
717 Messungen und Beobachtungen, in: *Klimabericht für die Metropolregion Hamburg*, edited by: von Storch, H. and
718 Claussen, M., Springer, Berlin, Heidelberg, 19–59, https://doi.org/10.1007/978-3-642-16035-6_2, 2011.

719 Rosentreter, J. A., Wells, N. S., Ulseth, A. J., and Eyre, B. D.: Divergent Gas Transfer Velocities of CO₂, CH₄,
720 and N₂O Over Spatial and Temporal Gradients in a Subtropical Estuary, *J. Geophys. Res. Biogeosciences*, 126,
721 e2021JG006270, <https://doi.org/10.1029/2021JG006270>, 2021.

- 722 Sanders, T., Schöl, A., and Dähnke, K.: Hot Spots of Nitrification in the Elbe Estuary and Their Impact on Nitrate
723 Regeneration, *Estuaries Coasts*, 41, 128–138, <https://doi.org/10.1007/s12237-017-0264-8>, 2018.
- 724 Scharfe, M., Callies, U., Blöcker, G., Petersen, W., and Schroeder, F.: A simple Lagrangian model to simulate
725 temporal variability of algae in the Elbe River, *Ecol. Model.*, 220, 2173–2186,
726 <https://doi.org/10.1016/j.ecolmodel.2009.04.048>, 2009.
- 727 Schoer, J. H.: Determination of the origin of suspended matter and sediments in the Elbe estuary using natural
728 tracers, *Estuaries*, 13, 161–172, <https://doi.org/10.2307/1351585>, 1990.
- 729 Schöl, A., Hein, B., Wyrwa, J., and Kirchesch, V.: Modelling Water Quality in the Elbe and its Estuary – Large
730 Scale and Long Term Applications with Focus on the Oxygen Budget of the Estuary, *Küste*, 203–232, 2014.
- 731 Schroeder, F.: Water quality in the Elbe estuary: Significance of different processes for the oxygen deficit at
732 Hamburg, *Environ. Model. Assess.*, 2, 73–82, <https://doi.org/10.1023/A:1019032504922>, 1997.
- 733 Sharma, N., Flynn, E. D., Catalano, J. G., and Giammar, D. E.: Copper availability governs nitrous oxide
734 accumulation in wetland soils and stream sediments, *Geochim. Cosmochim. Acta*, 327, 96–115,
735 <https://doi.org/10.1016/j.gca.2022.04.019>, 2022.
- 736 Siedler, G. and Peters, H.: Properties of sea water, Physical properties, in: *Oceanography*, vol. V/3a, edited by:
737 Sündermann, J., Springer, Berlin, Germany, 233–264, 1986.
- 738 Silvennoinen, H., Hietanen, S., Liikanen, A., Stange, C. F., Russow, R., Kuparinen, J., and Martikainen, P. J.:
739 Denitrification in the River Estuaries of the Northern Baltic Sea, *AMBIO J. Hum. Environ.*, 36, 134–140,
740 [https://doi.org/10.1579/0044-7447\(2007\)36\[134:DITREO\]2.0.CO;2](https://doi.org/10.1579/0044-7447(2007)36[134:DITREO]2.0.CO;2), 2007.
- 741 Sommerfield, C. K. and Wong, K.-C.: Mechanisms of sediment flux and turbidity maintenance in the Delaware
742 Estuary, *J. Geophys. Res. Oceans*, 116, C01005, <https://doi.org/10.1029/2010JC006462>, 2011.
- 743 Tang, W., Tracey, J. C., Carroll, J., Wallace, E., Lee, J. A., Nathan, L., Sun, X., Jayakumar, A., and Ward, B. B.:
744 Nitrous oxide production in the Chesapeake Bay, *Limnol. Oceanogr.*, 67, 2101–2116,
745 <https://doi.org/10.1002/lno.12191>, 2022.
- 746 Tian, H., Xu, R., Canadell, J. G., Thompson, R. L., Winiwarter, W., Suntharalingam, P., Davidson, E. A., Ciais,
747 P., Jackson, R. B., Janssens-Maenhout, G., Prather, M. J., Regnier, P., Pan, N., Pan, S., Peters, G. P., Shi, H.,
748 Tubiello, F. N., Zaehle, S., Zhou, F., Arneeth, A., Battaglia, G., Berthet, S., Bopp, L., Bouwman, A. F., Buitenhuis,
749 E. T., Chang, J., Chipperfield, M. P., Dangal, S. R. S., Dlugokencky, E., Elkins, J. W., Eyre, B. D., Fu, B., Hall,
750 B., Ito, A., Joos, F., Krummel, P. B., Landolfi, A., Laruelle, G. G., Lauerwald, R., Li, W., Lienert, S., Maavara,
751 T., MacLeod, M., Millet, D. B., Olin, S., Patra, P. K., Prinn, R. G., Raymond, P. A., Ruiz, D. J., van der Werf, G.
752 R., Vuichard, N., Wang, J., Weiss, R. F., Wells, K. C., Wilson, C., Yang, J., and Yao, Y.: A comprehensive
753 quantification of global nitrous oxide sources and sinks, *Nature*, 586, 248–256, <https://doi.org/10.1038/s41586-020-2780-0>, 2020.
- 755 US EPA: Volunteer Estuary Monitoring: A Methods Manual, United States Environmental Protection Agency
756 (EPA), 2006.
- 757 Walter, S., Bange, H. W., and Wallace, D. W. R.: Nitrous oxide in the surface layer of the tropical North Atlantic
758 Ocean along a west to east transect, *Geophys. Res. Lett.*, 31, L23S07, <https://doi.org/10.1029/2004GL019937>,
759 2004.
- 760 Wanninkhof, R.: Relationship between wind speed and gas exchange over the ocean, *J. Geophys. Res. Oceans*, 97,
761 7373–7382, <https://doi.org/10.1029/92JC00188>, 1992.
- 762 Weiss, R. F.: The solubility of nitrogen, oxygen and argon in water and seawater, *Deep Sea Res. Oceanogr. Abstr.*,
763 17, 721–735, [https://doi.org/10.1016/0011-7471\(70\)90037-9](https://doi.org/10.1016/0011-7471(70)90037-9), 1970.
- 764 Weiss, R. F. and Price, B. A.: Nitrous oxide solubility in water and seawater, *Mar. Chem.*, 8, 347–359,
765 [https://doi.org/10.1016/0304-4203\(80\)90024-9](https://doi.org/10.1016/0304-4203(80)90024-9), 1980.

- 766 Wells, N. S., Maher, D. T., Erler, D. V., Hipsey, M., Rosentreter, J. A., and Eyre, B. D.: Estuaries as Sources and
767 Sinks of N₂O Across a Land Use Gradient in Subtropical Australia, *Glob. Biogeochem. Cycles*, 32, 877–894,
768 <https://doi.org/10.1029/2017GB005826>, 2018.
- 769 Wertz, S., Goyer, C., Burton, D. L., Zebarth, B. J., and Chantigny, M. H.: Processes contributing to nitrite
770 accumulation and concomitant N₂O emissions in frozen soils, *Soil Biol. Biochem.*, 126, 31–39,
771 <https://doi.org/10.1016/j.soilbio.2018.08.001>, 2018.
- 772 de Wilde, H. P. and de Bie, M. J.: Nitrous oxide in the Schelde estuary: production by nitrification and emission
773 to the atmosphere, *Mar. Chem.*, 69, 203–216, [https://doi.org/10.1016/S0304-4203\(99\)00106-1](https://doi.org/10.1016/S0304-4203(99)00106-1), 2000.
- 774 Winterwerp, J. C. and Wang, Z. B.: Man-induced regime shifts in small estuaries—I: theory, *Ocean Dyn.*, 63,
775 1279–1292, <https://doi.org/10.1007/s10236-013-0662-9>, 2013.
- 776 WMO: Scientific Assessment of Ozone Depletion: 2018, World Meteorological Organization, Geneva,
777 Switzerland, 2018.
- 778 Wolfstein, K. and Kies, L.: Composition of suspended particulate matter in the Elbe estuary: Implications for
779 biological and transportation processes, *Dtsch. Hydrogr. Z.*, 51, 453–463, <https://doi.org/10.1007/BF02764166>,
780 1999.
- 781 Wrage, N., Velthof, G. L., van Beusichem, M. L., and Oenema, O.: The role of nitrifier denitrification in the
782 production of nitrous oxide, *Soil Biol. Biochem.*, 33, 1723–1732, [https://doi.org/10.1016/S0038-0717\(01\)00096-](https://doi.org/10.1016/S0038-0717(01)00096-7)
783 7, 2001.
- 784 Zander, F., Heimovaara, T., and Gebert, J.: Spatial variability of organic matter degradability in tidal Elbe
785 sediments, *J. Soils Sediments*, 20, 2573–2587, <https://doi.org/10.1007/s11368-020-02569-4>, 2020.
- 786 Zander, F., Groengroeft, A., Eschenbach, A., Heimovaara, T. J., and Gebert, J.: Organic matter pools in sediments
787 of the tidal Elbe river, *Limnologica*, 96, 125997, <https://doi.org/10.1016/j.limno.2022.125997>, 2022.
- 788 ZDM: Abfluss - Neu Darchau, edited by: Wasserstraßen- und Schifffahrtsamt Elbe, 2022.